МОСКОВСКИЙ
ОРДЕНА ТРУДОВОГО
КРАСНОГО ЗНАМЕНИ
ИНЖЕНЕРНО-
ФИЗИЧЕСКИЙ ИНСТИТУТ

003-94

BENCHMARK-EXPERIMENTS AND ANALYSES ON STREAMING OF 14-MEV NEUTRONS IN IRON AND IRON-WATER RADIATION SHIELDING MOCK-UPS WITH SLITS

Moscow 1994

State Higher Education Committee of Russian Federation

Moscow Engineering Physics Institute
(Technical University)

BENCHMARK-EXPERIMENTS AND ANALYSES ON STREAMING OF 14-MEV NEUTRONS IN IRON AND IRON-WATER RADIATION SHIELDING MOCK-UPS WITH SLITS

PREPRINT 003-94

Approved by Editorial Board of the Institute

Moscow 1994

UDK 621.039.5

BENCHMARK-EXPERIMENTS AND ANALYSES ON STREAMING OF 14-MEV NEUTRONS IN IRON AND IRON-WATER RADIATION SHIELDING MOCK-UPS WITH SLITS

V.V.Afanasiev, M.I.Andreev, A.G.Belevitin, V.L.Romodanov,
Moscow Engineering Physics Institute, Russia, Moscow

D.V.Markovskij, A.N.Svetchkopal
The Russian Research Centre "Kurchatov Institute", Russia, Moscow

M.: Preprint/MEPhI, 004-94, 1994. - 52 p.

The experiments on measurements of absolute threshold reactions rates $^{237}Np(n,f)$, $^{115}In(n,n')$, $^{56}Fe(n,p)$, $^{63}Cu(n,2n)$ and gamma-ray doze rates, measured with thermoluminiscent detectors (TLD) of type $CaSO_4$ and $SrSO_4$, in the models of iron and iron-water radiation shield of fusion reactor with central and asymmetric slits are described. A neutron generator was used as a source of neutrons of reaction $T(d,n)^4He$. The experiments were calculated with the transport codes MCNP and BLANK. A consent of calculations with the experiment is demonstrated within the measurement errors.

ISBN 5-7262-0026-8

Introduction

Any design of the fusion reactor radiation shield usually has local heterogeneity, consisting of voids or inclusions of materials different from the bulk shield composition, provided for accommodation of plasma heating and pumping devices, diagnostics, cooling channels and in other design purposes. A heterogeneity of shield, as a rule, is accompanied by significant deterioration of its characteristics in comparison with a bulk shield, that requires the acceptance of additional measures on reductions of irradiation behind the shield to allowable levels. In conditions of compact geometry, typical for fusion reactors, an opportunity to provide the redundant thickness of additional shield in locations of heterogeneous fragments for compensation of possible calculational uncertainty is usually limited. Therefore to the accuracy of heterogeneous radiation shield calculations the high requirements (about tens of percents) are demanded.

It is known, that the direct test of characteristics of radiation shield in the fusion reactor conditions is impossible, until the first test fusion reactor will be constructed and put into operation. Therefore on a stage of designing such reactor (ITER) a verification of using transport codes and neutron data should be searched for in settlement and analysis of special "conceptual" benchmark-experiments with neutron generator, as a source of 14 MeV neutrons, and radiation shielding mock-ups which simulate the characteristic effects of neutron and γ-ray transport.

One of the typical in this sense characteristic models [1,2] is a radiation shield with longitudinal slit, in respect to direction of 14-Mev neutrons streaming, appropriate to structural backlashes of width 5 - 20 mm in vacuum vessel and radiation shield of reactor. As typical ones, two materials may be considered: pure

structural material (vacuum vessel) and structural material with a fraction of water of ~20 % (radiation shield). Stainless steel serves as a structural material in a majority of the known projects of fusion reactors.

In a given work the slit-models with material compositions of the both mentioned types on a basis of iron at total thickness of 400 mm were studied. The chosen thickness approximately corresponds to the structure accepted in previous conceptual design of ITER [3]. For a detailed comparative study of the slit-effect the different variants of the mock-up geometry (fig. 1) were considered: uniform one (without slit), with a straight slit of different width through all the shield, with a half-slit (a slit of 20 mm width in back half of the shield) and with a shifted slit of width 20 mm (with a shift of its halves in cross direction of the mock-up on 20 and 60 mm).

Experimental studies were done to order of the RRC "Kurchatov institute". A general guidance of the work and calculational analysis were provided by specialists of RRC. The experimental researches and necessary methods development were carried out by specialists of the "Neutron generator" laboratory of MEPhI.

Experimental assembly

The shielding mock-ups were assembled from rectangular blocks of sizes 25x200x500 mm from steel with contents of 98.7 % of iron. The material contents of impurity is given in table 1 (an error of elements contents is equal 30 %).

Table 1. The impurity contents in steel blocks of the mock-up.

Element	Na	Mg	S	Cl	V	Cr	Mn	Co
	Ni	Cu	Zn	O	C	N	Si	
Contents (%)	3.66-3	4.41-4	7.74-2	3.51-3	4.48-4	1.87-1	8.81-1	1.46-2
	3.68-1	4.69-2	7.29-3	<10-3	<10-3	<10-3	<10-3	

A general view of the mock-up is shown on fig. 2. The mock-up was assembled with overlapping of blocks in adjacent layers with the purpose of exception direct streaming of neutrons through possible backlashes between blocks. For suppression of background of neutrons, scattered by the walls of experimental hall, a neutron source shield was installed around the neutron generator target, which represented rectangular assembly from iron of approximate thickness ~250 mm with a conic aperture, directed towards experimental assembly. The source shield was surrounded by borated polyethylene for absorption of moderated neutrons. The neutron generator target in all experiments was installed at a distance 150 mm from the front mock-up surface. The structure of the target unit is described in [4].

An iron-water mock-up consists of alternate layers of iron and plex (polymethylmetacrilate) blocks for imitation of typical iron and hydrogen nuclei ratio in a composition of fusion reactor radiation shield. The average volume fractions of steel, plex and void in the mock-up are correspondingly 74.08 %, 25.28 % and 0.64 %. The material contents of plex is given in table 2. The outline of experimental installation is shown on fig. 3.

Table 2. Nuclear densities of plex components, $1/cm^3 \times 10^{22}$ (chemical formula $CH_2=C(CH_3)-COOCH_3$).

H	C	O
5.69	3.55	1.42

Measurement techniques

The following neutron and gamma fields functionals were measured in the experiments:

- reaction rates of threshold nuclear reactions $^{237}Np(n,f)$, $^{115}In(n,n')$, $^{56}Fe(n,p)$, $^{63}Cu(n,2n)$;
- absorbed doze rates in mixed neutron and gamma fields with help of thermoluminiscent detectors of type $CaSO_4$ and $SrSO_4$.

All the measurements were normalised to one source neutron. The average neutron generator yield in conducted measurements was 2×10^{10} s^{-1} at accelerating voltage 150 kV..

The activation measurements were conducted in two stages. On the first stage the absolute values of all threshold reactions rates on a front surface of the shielding mock-ups were determined. For that purpose disc detectors of diameter 18 mm and thickness 0.4-1 mm, made of one-isotope materials, were used. On the second stage the relative distributions of activation rates inside the mock-ups and on their back surface were measured and then normalised to the source neutron. The relative distributions of nuclear reactions rates on back surface of the mock-ups were measured with help of detectors from chemically pure materials in form of parallelepiped of sizes 2x5x30 mm, turned to the mock-up surface by side 2x30 mm. The application of such detectors is stipulated by large neutron field gradients near to slit in the mock-up. For detectors of different form and each kind of reaction the calibrations of γ-spectrometer were carried out.

The solid-state track detectors consisted of the layers ^{237}Np, put on aluminum foil of thickness 0.1 mm and sizes 5x8 mm. The number of nuclei in detectors made 4×10^{17}. An aluminum foil was bent, afterwards that the detector had a size 2.5x5 mm. An absolute calibration of detectors was conducted by their irradiation in certificated neutron field of neutron generator together with earlier calibrated similar detectors.

The chosen for measurements threshold detectors are sensitive to neutrons in different regions of the total 1-15 MeV energy range (fig. 4). In that sense one may consider them as representing neutron flux in some groups of that range.

For measurement of the doze rate characteristics of neutron and gamma fields the thermoluminiscent detectors of $CaSO_4$ and $SrSO_4$ types were irradiated in the mock-ups. Choosing of these detectors pursuant to techniques [6] permits to interpolate the γ-heating in iron depending on effective atomic number. The calibration

of detectors was conducted in certificated γ-field from the source ^{137}Cs with the energy 661.5 keV at a point with absorbed doze rate in air (0.133+0.009) mrad/s.

The detectors represented glass ampoules with thickness of walls of 0.5 mm, in which the powder of thermoluminiscent material is packed. An active part of detector is a cylinder with a diameter 1 mm and a length 20 mm. It was shown in special measurements, that the glass of ampoule does not give contribution to the glowing of detector. For measurement of thermo-glowing the installation of type Harshaw-2080 was used. Some properties of the detectors used in experiments are given in table 3.

The used method of neutron- and γ-ray-components separation in the absorbed TLD dose rate corresponds to the works [5,6]. The neutron spectra were taken from BLANK [7] calculations. For estimation of absorbed dose rate in iron a linear interpolation on effective atomic numbers of the detectors $CaSO_4$ and $SrSO_4$ was used. It was shown that the use of ^{137}Cs γ-source instead of ^{60}Co for calibration of the γ-dose rate in air results in error on a level of 8%.

The error components of absolute γ-heating measurements in neutron- and γ–fields with TLD are given in table 4.

The total error of experimental absorbed γ-ray dose rate in iron is estimated as 50%.

Table 3. Main characteristics of TLD*.

Characteristics	The type of detector	
	$CaSO_4$	$SrSO_4$
Effective atomic number	15.2	30.0
Detector mass, g	5 - 8	6 - 10
Temperature of heating before irradiation, °C	300	400
Duration of heating, min.	15	15
Limits of the glowing curve integration, °C	90 - 230	90 - 260
Density, g/cm^3	2.96	3.96
Weight fractions of components	Ca - 0.294 S - 0.235 O - 0.470	Sr - 0.477 S - 0.175 O - 0.348

* The TLDs were manufactured by Moscow University specialists.

Table 4. Error components of γ-dozes measurements with TLD.

Error component	The type and value of error	
	Systematic	Statistical
Neutron yield per α-particle	2.7	-
Fluence of α-particles	-	0.2
Distance from neutron source to the mock-up front surface	1.3	-
Absolute calibration of TLD	10.0	-
Integration of the thermal glowing curve area	-	2-10
Coordinate of detector position	2-7	-
Detector mass	1.5	-
Use of calculated neutron spectra	20	-
Linearity of interpolation on effective atomic number	20	-
Account of detector fading	2	-
Background of glowing	2	-

Because of some deuteron beam smearing, in experiments with a slit 5 mm wide it is necessary to limit a size of active target spot, visible through the slit, so that all it was inside the slit size in view of possible uncertainty of the beam position and had approximately uniform distribution of neutron density, assumed in the calculations. In auxiliary calculations and experiments it was shown, that in the mock-up with a slit width 5 mm the diameters of the target active spot should not exceed 3 mm. For that on a way of deuteron beam a slit diaphragm 3 mm wide was installed. In measurements with the slit width 20 mm this effect was not observed, that is confirmed experimentally in measurements with diaphragm and without it.

Calculational method

The calculations of threshold detectors activation rates in experimental mock-up were carried out with 3-D codes BLANK and MCNP. The γ-ray nuclear heating distributions (an absorbed doze rate in iron component of assembly) were calculated with MCNP. For calculation of neutron fluxes in both codes the local estimation in points on the mock-up axis and on its back surface was used. The BLANK code for neutron transport calculations uses the library of working constants, processed from the ENDF/B-4 data files. An activation cross-sections of threshold detectors were taken from the library [8] (fig. 4). In MCNP code the neutron data with point-wise representations of cross-sections on a basis of ENDL-85 files were used.

In calculations with MCNP code the real geometry of the model was preset. In the BLANK code the model geometry was presented in kind rectangular prism, and

the neutron source shield, having a conical aperture, was simplified to stepped composition (fig. 5).

In both calculations the statistics made a few millions of histories, that corresponds to the errors of neutron spectra within ~10 %.

The results and comparison

The numerical results of experiments with all the shielding compositions are given in tables 5-10. Below they are discussed in comparison with the calculations.

Iron shield

The results of activation rates measurements in shielding compositions from iron in comparison with calculations with the codes BLANK and MCNP are given on fig. 6-29. The results are shown on drawings simultaneously in points on the mock-up central axis and then in the same scale on its back surface in cross direction along the slit shift.

On fig. 6-13 the results for each of threshold detectors activation rates, presenting appropriate neutrons energy ranges, for a straight slits of width 5 and 20 mm are shown. As a whole, the results of calculations with the codes BLANK and MCNP are in good agreement among themselves and with the experiment, as on shield thickness, as on its back surface. The exceptions make the divergence of activation rates for the low-threshold detectors (In and Np) on the mock-up front wall in calculations with code BLANK and in both calculations on the mock-up back surface. In the first case it could be explained by simplified form of internal cavity of the source shield in calculations with code BLANK, and in the second case by presence of background scattered neutrons in experimental hall, not taken into account in calculations.

The same results for each detector are shown on fig. 14-17 in dependence on a slit width. For high-threshold detectors (Cu and Fe), sensitive to the fast component of neutron spectrum, the attenuation factor of activation rates on thickness of the shield makes approximately three orders. The presence of any considered slits increases activation rates on exit from the slit approximately by 200 times in comparison with the uniform shield. This peak on the back surface descends in cross direction to a level, appropriate to uniform shield, on a distance from the slit axis of order 50 mm for the slit width 5 mm and 100 mm for the slit 20 mm. For detectors with thresholds near ~1 MeV (In and Np) the activation rates descend along the shield thickness on two orders, that is explained by accumulation of the soft component in neutron spectrum along the shield thickness. For these detectors a small increase (on 30 - 50 %) of the activation rates on exit from the slit at increase its width from 5 to 20 mm can be noticed.

The distributions of activation rates for a shift of 20 mm slit in back half of the assembly in cross direction on 20 and 60 mm are given on fig. 18-25. Here a good consent of BLANK and MCNP calculations among themselves and with experiment can also be noted. On fig. 26-29 these results are compared at different values of the slit shift. It is visible, that for all the detectors the cross shift of a slit on a size of its width is not followed by considerable reduction of the neutron flux values in the neutron energy range to ~1 MeV. At a shift of slit axis on 60 mm approximately the

equal peaks on exits from the shield are seen in cross direction of assembly opposite to slit axes in front and back its halves, between which the minimum, equal approximately to half of the peak value presents. For detectors with high threshold the peak value is approximately on two orders lower than on exit from straight slit. For detectors with low threshold the total effect of straight slit makes whole one order, and a shift of half-slit in cross direction reduces the peak value of scattered neutrons flux in several times. The latter, obviously, is explained by small contribution in activation of these detectors of the source neutrons and multi-scattering of moderated neutrons before their leakage from the assembly. The peak values of activation rates on fig. 10-13 for a slit 20 mm wide in the back half of the shield agrees with corresponding maximal values on fig. 18-21 for a slit shifted on 60 mm.

A comparison of the γ-ray absorbed dose rate distributions is shown on fig. 30 for a bulk shield and a shield with a straight slit 20 mm wide. The results measured with TLD are in good (within ~10%) agreement with the MCNP calculation, as on the thickness of the bulk shield as on the back surface of the shield with slit. The γ-ray absorbed dose rate descends along the thickness of the bulk shield in ~500 times. As it may be expected, introducing in a shield of a straight slit 20 mm wide makes significantly lower effect in increasing of the absorbed γ-ray dose rate at the slit exit (4-5 times), than for the fast neutrons.

It is known, that in the used experimental technique the determination of γ-doze rate is based on subtraction from the detector total light yield of the part, appropriate to neutrons, which is determined in calculation. The error of estimation of the neutron component of the light yield is difficult to determine, as it includes not only the errors of nuclear constants (kerma-factors, electrons stop energy etc.), but also calculated spectra of neutron fluxes in points of detectors location. The value of this component and its ratio to the γ-component considerably vary on thickness of uniform assembly, as well as in dependence on slit arrangement, as a result of exposition of detector by primary source neutrons with the energy near 14 MeV. The least error of technique, thus, corresponds to cases of measuring points location in depth of uniform shield or at some distance from the slit exit, where the neutron component is much lower than γ-component. That results also in decreasing the difference of measurements with detectors having different atomic numbers at movement in the depth of the shield, noticeable on fig. 30. Another problem corresponds to γ-dose measurements with TLD in voids where the method is not directly applied.

Iron-water shield

An experiments on the iron-water shielding mock-up were carried out for a straight slit of width 20 mm. The results of calculations are compared with experiment on fig. 31-34. Owing to lower (on ~20 %) iron contents at the same shield thickness the attenuation of the neutron flux of the source group at the exit from such bulk shield is lower, than for an iron shield, that is displayed in reduction of attenuation of activation rates of Cu and Fe detectors approximately twice. For In and Np detectors the attenuation factor in iron-water assembly is approximately the same, as in the assembly from iron. From figures it follows, that the peak values of the detectors activation rates at the slit exit and the curves along the shield back surface are in good (within the limits of 10 %) agreement with the experiment.

A comparison of the absorbed gamma-ray dose rates is given on fig.35. As a whole, the character of consent corresponds to the results on fig. 30 for an iron shield.

Conclusions

The carried out experimental and calculational studies of the key iron and iron-water shielding compositions with slits, recommended for testing of transport codes and neutron data in frameworks of project ITER [2], let us make the following main conclusions:

1. The results of calculations with codes BLANK and MCNP of activation rates distributions for four threshold detectors, presenting characteristic groups in the neutron energy range 1-14 MeV, are in good (within the error of measurements ~10%) agreement with experiment as on shielding compositions thickness, as on its back surface in cross direction to the slit. That gives a basis to assume, that in reactor calculations for considered shield thickness the spectral components of the neutron flux are reproduced with similar accuracy in estimates of nuclear heating, stipulated by neutrons, and of neutron doze for similar shield with slits.

2. The carried out MCNP calculations of γ-heating distributions in uniform iron shield and composition with a straight slit of the width 20 mm also agree (within ~10%) with measurements of absorbed doze rates in iron with help of thermoluminiscent dosimeters.

3. Estimating the characteristic values of the effects of slit introduction in uniform iron shield of thickness 400 mm (as well as in iron-water shield), one may note, that the presence of straight longitudinal slit of the width even 5 mm in considered configuration of the model with the neutron source placed on its axis results in increase of neutron flux in the energy group of the source at the exit from the slit on two orders in comparison with the values for uniform shield. For all considered threshold detectors the cross shift of half of shield on size of the slit width does not result in considerable reduction of neutron peak flux in the energy range up to ~1 MeV. At a shift of slit axis on 60 mm approximately the equal peak values of neutrons flux at exits from the shield are appeared in cross direction of the assembly opposite to slits axes, between which the minimum, equal approximately to half of the peak value presents. For detectors with high threshold (Cu and Fe) the peak value is approximately by two orders lower than that at the exit from a straight slit. For detectors with low threshold (In and Fe) the total effect of a straight slit makes whole one order, and at a shift of slit fragment in cross direction the peak value of scattered neutrons flux decreases in several times.

4. An important conclusion of conducted work is the necessity of the experimental techniques perfection for nuclear heating measurements, stipulated by neutrons and γ-rays, for more reliable estimation of calculated components of techniques, as well as development, whenever possible, of the measurement philosophy, not relying on using calculated values.

References

1. D.V.Markovskij, A.N.Svetchkopal. Shielding experiments and analysis for substantiation of CTR projects. ITER Experts Meeting on Shielding Experiments and Analysis. ITER-IL-BL-4-0-6, 1990.
2. Summary report of ITER Expert Meeting on Shielding Experiments and Analysis.
   ITER-IL-BL-5-0-5, Feb. 1990.
3. ITER Concept Definition, Vol.1,2. ITER documentation series, No.3., IAEA, Vienna, 1989.
4. V.V.Afanasiev et al. Benchmark experiments and analysis with hybrid reactor mock-ups. Preprint MEPhI 003-92, 1992.
5. H.Hashikura et al. Calculation of neutron response of thermoluminiscent dosimeters. J. of Faculty of Eng., the University of Tokio, vol. XXXIX, No 1(1987), 7-16.
6. S.Tanaka, N.Sasamoto. Gamma-ray absorbed dose measurement in media with thermoluminiscent dosimeters having different atomic numbers. J. of Nucl. Sci. & Techn., 22(2), February 1985, 109-119.
7. S.V.Marin, D.V.Markovskij, G.E.Shatalov. Preprint KIAE-2382, 1977.
8. A.A.Lapenas. The library of threshold reactions group cross sections (BGS-1). Proc. of conf. "Metrology of neutron measurements in nuclear-physical installations", v.1, M.: 1976 (in Russian)

Table 5. Reaction rates in composition 1 (iron bulk shield).

Coordinate, mm	Reaction			
	$^{63}Cu(n,2n)$	$^{56}Fe(n,p)$	$^{115}In(n,n')$	$^{237}Np(n,f)$
	Along Y axis (*10^{27} /neutron/nucleus)			
0	0.191(8)	0.040(2)	0.094(5)	1.50(16)
50	0.060(4)	0.0133(5)	0.067(4)	0.85(9)
100	0.0208(15)	0.0048(2)	0.035(2)	0.47(5)
150	0.0077(6)	0.00187(8)	0.0179(11)	0.27(3)
200	0.0032(2)	0.00074(4)	0.0090(6)	0.16(2)
250	0.00122(9)	0.00031(2)	0.0044(3)	0.095(11)
300	0.00049(4)	0.000117(6)	0.00213(14)	0.059(7)
350	0.000195(15)	0.000052(4)	0.00103(7)	0.031(4)
400	0.000079(6)	0.000023(2)	0.00038(3)	0.0125(14)
	Along X axis (*10^{31} /neutron/nucleus)			
0	0.79(6)	0.226(12)	3.8(3)	142(16)
8	0.78(5)	0.221(12)	4.8(4)	133(16)
12	0.74(5)	-	5.1(5)	136(16)
16	0.78(5)	0.197(11)	4.8(4)	134(16)
20	0.78(5)	0.201(11)	4.4(4)	126(16)
32	0.74(5)	0.209(12)	4.4(4)	135(16)
52	0.71(5)	0.193(12)	4.5(4)	137(16)
72	0.68(5)	0.176(11)	4.4(4)	128(16)

Table 6. Reaction rates in composition 2 (with a straight slit).

Coordinate, mm	Reaction			
	$^{63}Cu(n,2n)$	$^{56}Fe(n,p)$	$^{115}In(n,n')$	$^{237}Np(n,f)$
	A slit 5 mm wide			
	Along Y axis (*10^{28} /neutron/nucleus)			
0	1.91(10)	0.42(2)	0.89(5)	
200	0.41(2)	0.084(3)	0.129(6)	
	Along X axis (*10^{28} /neutron/nucleus)			
0	0.145(6)	0.031(2)	0.0204(13)	0.8(1)
4	0.0084(9)	0.00214(16)	0.0057(3)	0.19(2)
8	0.00287(17)	0.00065(3)	0.0043(5)	0.16(2)
16	0.00180(10)	0.00042(2)	0.0045(3)	0.15(2)
32	0.00120(7)	0.000294(15)	0.0039(2)	0.132(16)
72	0.00082(6)	0.000206(18)	0.0033(2)	0.115(16)
	A slit 20 mm wide			
	Along Y axis (*10^{27} /neutron/nucleus)			
0	0.191(8)	0.043(2)	0.084(5)	1.34(15)
60	0.107(6)	0.025(1)	0.062(4)	0.97(11)
120	0.072(4)	0.0162(9)	0.036(2)	0.59(7)
180	0.046(3)	0.0097(6)	0.021(1)	0.42(5)
240	0.032(2)	0.0073(5)	0.0124(8)	0.27(3)
300	0.024(2)	0.0050(3)	0.0075(5)	0.18(2)
360	0.0191(13)	0.0040(3)	0.0049(4)	0.125(14)
400	0.0151(9)	0.0030(2)	0.0035(3)	0.101(12)
	Along X axis (*10^{28} /neutron/nucleus)			
0	0.151(9)	0.0327(11)	0.035(2)	0.96(11)
8	0.149(9)	0.0319(11)	0.033(2)	0.97(11)
12	0.030(2)	0.0071(3)	0.0154(10)	0.33(4)
16	0.0102(8)	0.00246(10)	0.0107(7)	0.216(25)
20	0.0064(5)	0.00157(8)	0.0087(6)	0.184(21)
32	0.0032(3)	0.00084(4)	0.0069(5)	0.159(17)
52	0.00181(15)	0.00046(2)	0.0056(5)	0.152(17)
72	0.00127(12)	0.00033(2)	0.0048(4)	0.129(14)

Table 7. Reaction rates in composition 3 (with a shifted slit 20 mm wide).

Coordinate, mm	Reaction			
	$^{63}Cu(n,2n)$	$^{56}Fe(n,p)$	$^{115}In(n,n')$	$^{237}Np(n,f)$
A shift of slit on 20 mm				
Along Y axis (*10^{28} /neutron/nucleus)				
0	1.91(8)	0.40(2)	0.83(5)	
200	0.055(3)	0.0125(9)	0.106(6)	
Along X axis (*10^{28} /neutron/nucleus)				
-48	0.0023(2)	0.00048(3)	0.0062(5)	0.163(18)
-30	0.0034(2)	0.00065(3)	0.0059(5)	0.166(18)
-20	0.0045(3)	0.00089(4)	0.0065(5)	0.169(19)
-14	0.0068(4)	0.00103(4)	0.0075(5)	0.179(20)
0	0.0077(5)	0.00108(6)	0.0085(6)	0.218(24)
6	0.0085(5)	0.00114(7)	0.0095(9)	0.196(24)
12	0.00220(13)	0.00294(12)	0.0122(10)	0.289(31)
14	0.0058(4)	-	-	0.45(5)
16	0.088(5)	0.0089(3)	0.0215(12)	0.55(6)
20	0.082(5)	0.0082(3)	0.0183(10)	0.45(5)
26	0.030(2)	0.0043(2)	0.0157(10)	0.311(35)
34	0.0126(8)	0.00235(9)	0.0114(7)	0.246(27)
48	0.0056(4)	0.00098(4)	0.0081(6)	0.194(22)
A shift of slit on 60 mm				
Along Y axis (*10^{28} /neutron/nucleus				
0	1.91(8)	0.40(2)	0.83(5)	
200	0.031(2)	0.0068(3)	0.080(5)	
Along X axis (*10^{28} /neutron/nucleus)				
-40	0.0028(2)	0.00065(3)	0.0059(4)	0.156(17)
-20	0.0048(3)	0.00106(7)	0.0064(7)	0.179(19)
-12	0.0073(4)	0.00146(6)	0.0067(7))	0.185(19)
0	0.0078(4)	0.00155(7)	0.0064(6)	0.192(20)
12	0.0075(4)	0.00140(6)	0.0062(7)	0.197(21)
20	0.0054(3)	0.00106(5)	0.0066(7)	0.188(20)
30	0.0038(2)	0.00080(4)	0.0064(5)	0.186(20)
40	0.0035(2)	0.00065(4)	0.0067(5)	0.194(21)
48	0.0036(2)	0.00074(4)	0.0081(6)	0.212(25)
60	0.0060(4)	0.00113(6)	0.0094(7)	0.240(27)
72	0.0058(4)	0.00116(7)	0.0081(6)	0.222(26)
85	0.0033(2)	0.00061(3)	0.0067(6)	0.180(18)
110	0.00155(9)	0.00031(3)	0.0046(5)	0.141(16)

Table 8. Reaction rates in composition 4 (with a slit in back half of the shield).

Coordinate, mm	Reaction			
	$^{63}Cu(n,2n)$	$^{56}Fe(n,p)$	$^{115}In(n,n')$	$^{237}Np(n,f)$
	Along Y axis (*10^{28} /neutron/nucleus)			
0	1.91(10)	0.41(3)	0.91(6)	
200	0.033(2)	0.0073(3)	0.136(9)	
	Along X axis (*10^{28} /neutron/nucleus)			
0	0.0072(5)	0.00150(6)	0.0154(11)	0.232(25)
6	0.0070(5)	0.00143(6)	0.0150(9)	0.233(25)
12	0.0034(2)	0.00075(3)	0.0126(8)	0.179(27)
20	0.00174(10)	0.00040(2)	0.0098(6)	0.151(17)
40	0.00103(8)	0.000267(14)	0.0069(5)	0.137(16)
72	0.00088(7)	0.000213(12)	0.0070(5)	0.124(14)

Table 9. Reaction rates in composition 5 (iron-water shield with a straight slit 20 mm wide).

Coordinate, mm	Reaction			
	$^{63}Cu(n,2n)$	$^{56}Fe(n,p)$	$^{115}In(n,n')$	$^{237}Np(n,f)$
	Along X axis (*10^{28} /neutron/nucleus)			
0	0.160(14)	0.032(2)	0.0317(12)	0.78(9)
12	0.041(3)	0.0094(5)	0.0124(7)	0.273(30)
16	0.0133(5)	0.08302(12	0.0083(3)	0.131(15)
20	0.0082(3)	0.00196(8)	0.0069(3)	0.095(11)
32	0.0042(2)	0.00114(5)	0.0048(2)	0.067(7)
72	0.00174(8)	0.00055(2)	0.00284(12)	0.043(5)
140	0.00113(6)	0.00033(2)	0.00183(9)	0.026(29)

Table 10. Neutron and γ-ray components of the absorbed dose rate in TLD and interpolated absorbed γ-dose rate in iron of the shield at compositions 1-3 ($*10^{-14}$ erg/g/neutron).

Coordinate, mm	$CaSO_4$		$SrSO_4$		Interpolation in iron
	n	γ	n	γ	γ
Composition 1 (along Y axis)					
0	2721(1306)	4232(2031)	846(406)	6331(3039)	5600(2920)
50	720(346)	2176(1044)	300(144)	2748(1319)	2540(1320)
100	250(120)	1016(487)	83.0(39.8)	1308(628)	1195(621)
150	138(66.2)	434(208)	52.0(25.0)	595(286)	535(278)
200	68.9(33.1)	202(97.0)	26.0(12.5)	270(130)	245(127)
250	30.0(14.4)	109(52.3)	18.0(8.6)	135(65.3)	125(65.0)
300	14.7(7.1)	60.7(29.1)	6.7(3.2)	73.3(35.2)	65.7(34.2)
350	6.6(3.2)	32.1(15.4)	3.7(1.8)	38.4(18.4)	35.0(18.2)
400	2.5(1.2)	13.3(6.4)	1.3(6.2)	15.7(7.5)	15.2(7.9)
Composition 2 with a slit 20 mm wide (along X axis)					
0	216(104)	99.0(47.5)	68.0(32.6)	232(111)	-
8	200(96)	82.0(39.4)	60.0(28.8)	253(121)	-
12	50.0(24)	101(49)	32.0(15.4)	123(59)	115(60)
16	20.2(9.7)	34.4(16.5)	6.9(3.3)	50.9(24.4)	45.0(23.4)
20	12.0(5.7)	27.2(13.1)	4.4(2.1)	39.9(19.2)	34.8(18.1)
32	8.8(4.2)	18.9(9.1)	3.1(1.5)	28.4(13.6)	24.8(12.9)
52	4.6(2.2)	17.2(8.3)	1.9(0.9)	22.0(10.6)	20.0(10.4)
72	3.5(1.7)	15.0(7.2)	1.5(0.7)	18.9(9.1)	17.2(8.9)
Composition 5 (along X axis)					
0	214(103)	190(99)	66.5(31.9)	231(120)	-
12	43.4(20.8)	124(65)	13.5(6.5)	104(52)	110(57)
16	23.5(11.3)	84.5(43.9)	7.4(3.6)	66.0(33.0)	72.2(37.5)
20	15.7(7.5)	74.1(38.5)	4.7(2.3)	58.6(29.3)	64.1(33.3)
32	7.3(3.5)	65.3(34.0)	2.2(1.1)	51.6(25.8)	56.0(29.1)
72	3.7(1.8)	49.8(25.9)	1.2(0.6)	37.0(18.5)	41.5(21.6)
140	2.26(1.09)	34.9(18.1)	0.6(0.3)	29.0(14.6)	31.0(16.1)

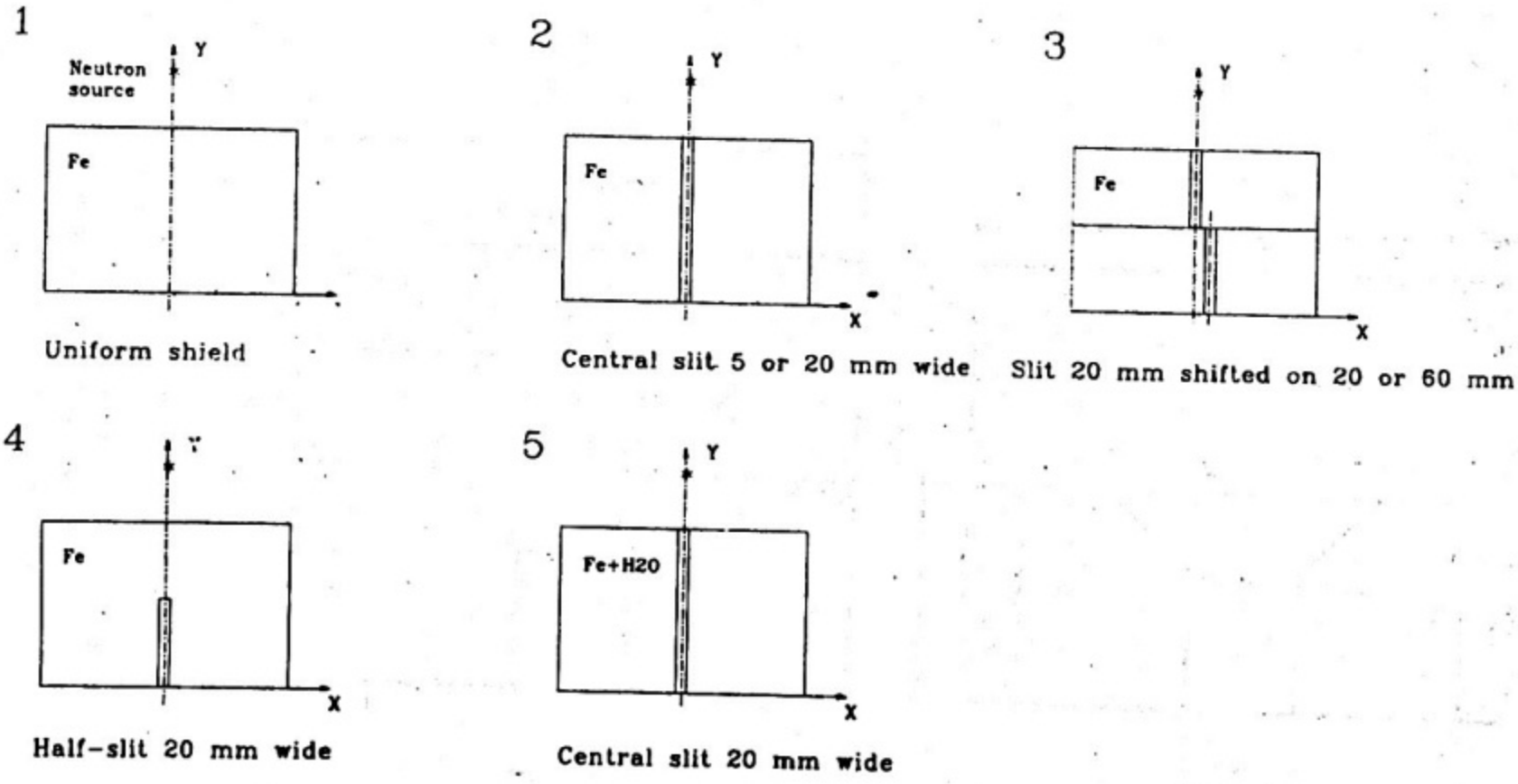

Fig. 1. Shielding compositions studied in the experiments.

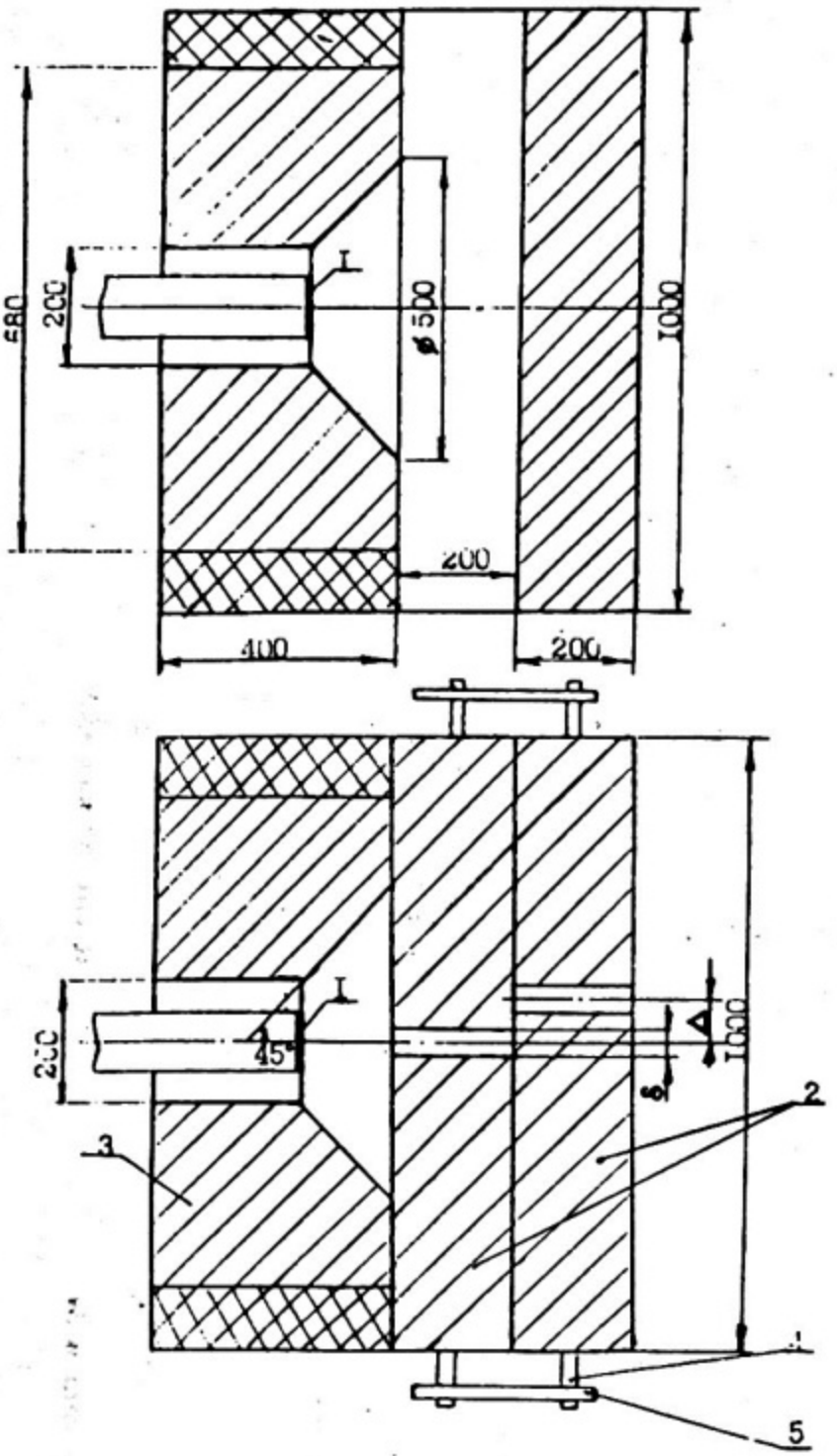

Fig. 2. A scheme of iron shielding mock-up.

▨ - Borated polyethylene, ▨ - Steel.
1 - Tritium target, 2 - Shielding mock-up, 3 - Source shield,
4 - Driving screw, 5 - Limiter, δ , Δ - varying parameters.

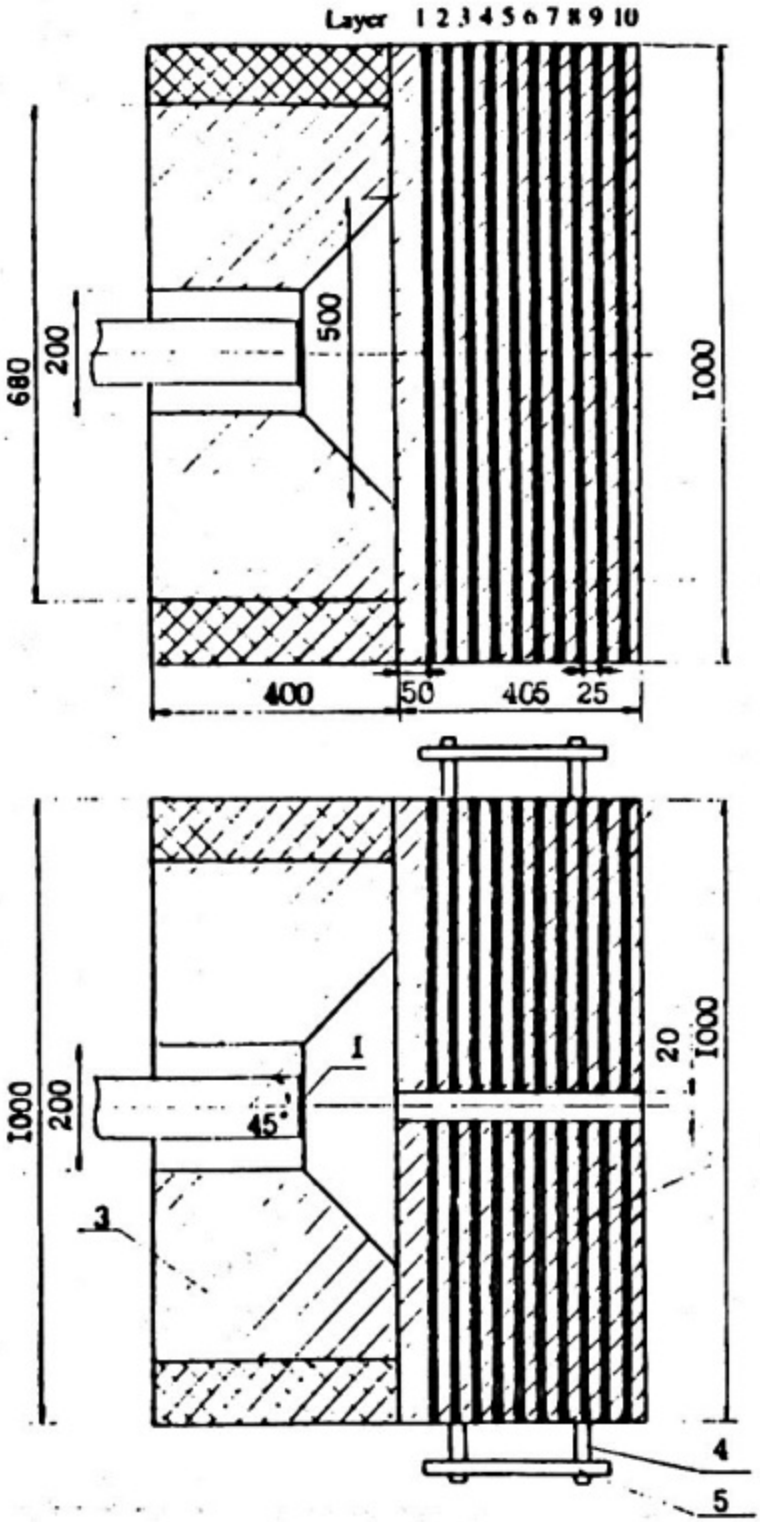

Layer	Thickness, mm
1	10.2
2	10.7
3	10.2
4	10.9
5	10.9
6	10.0
7	10.1
8	10.0
9	9.9
10	9.5

Fig. 3. A scheme of iron-water shielding mock-up.

▩ - Borated polyethylene, ▨ - Steel, ■ - Polymethylmetacrilate
1 - Tritium target, 2 - Shielding mock-up, 3 - Source shield,
4 - Driving screw, 5 - Limiter.

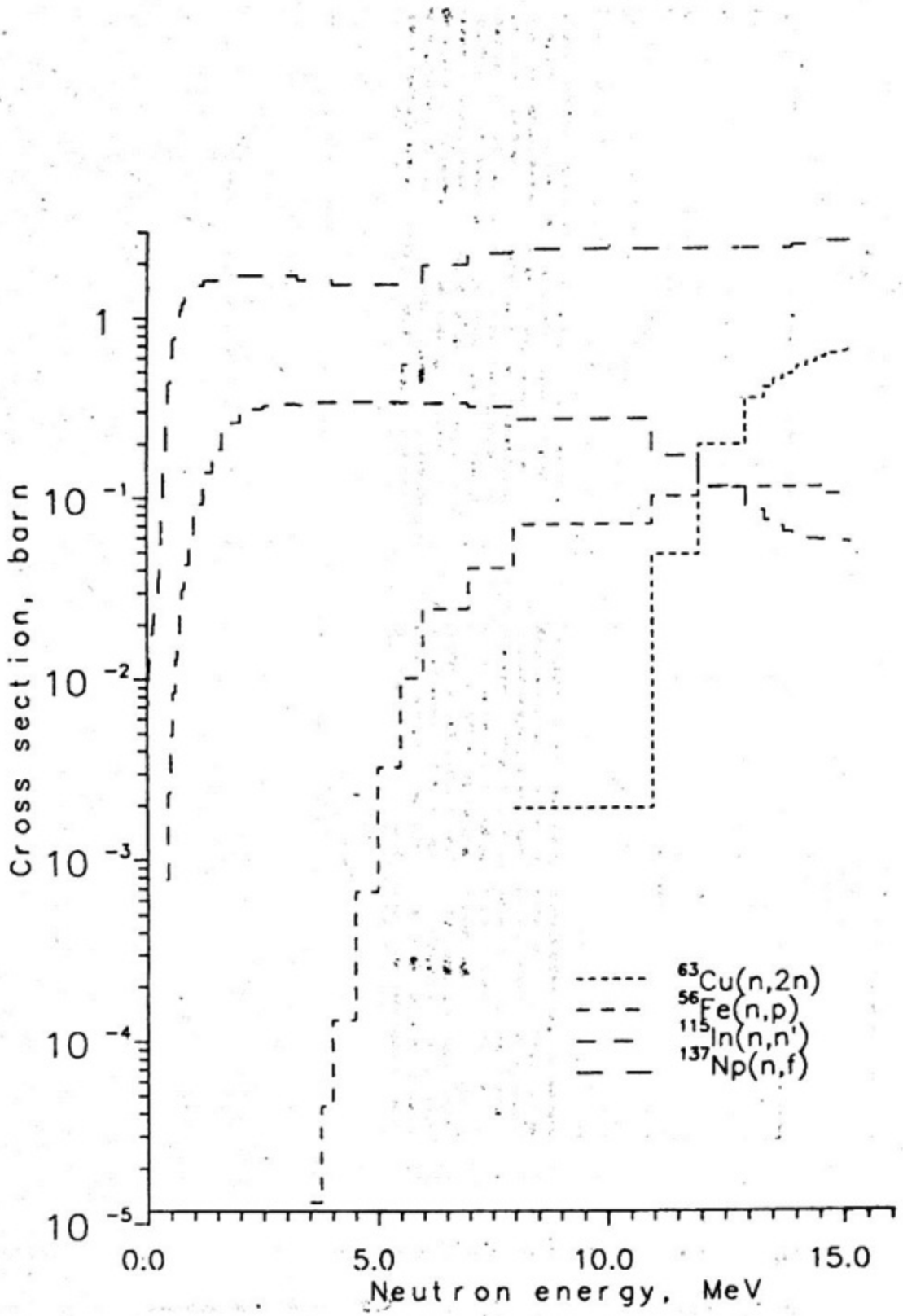

Fig. 4. Group cross sections of activation detectors in BLANK.

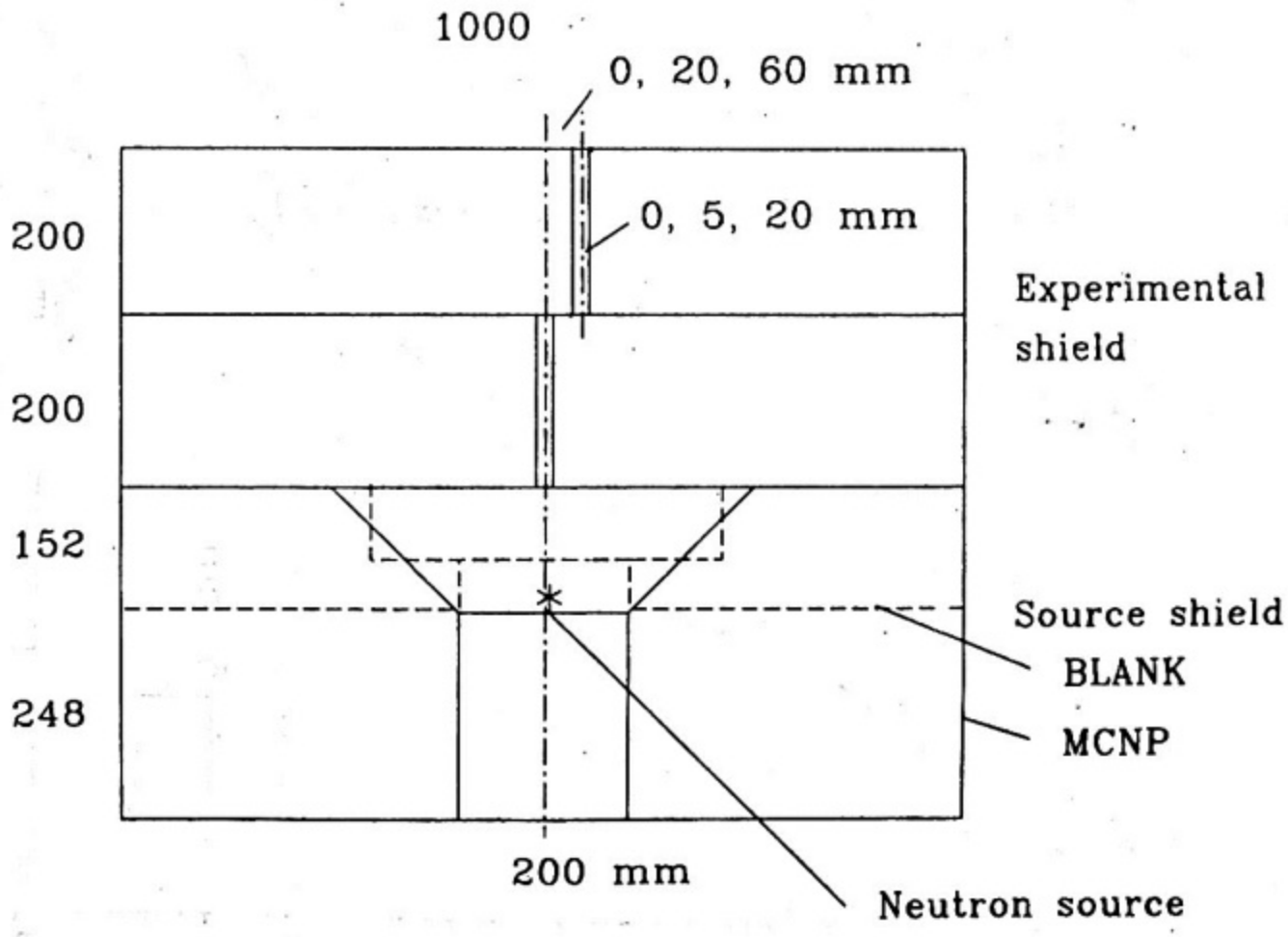

Fig. 5. A scheme of calculational model.

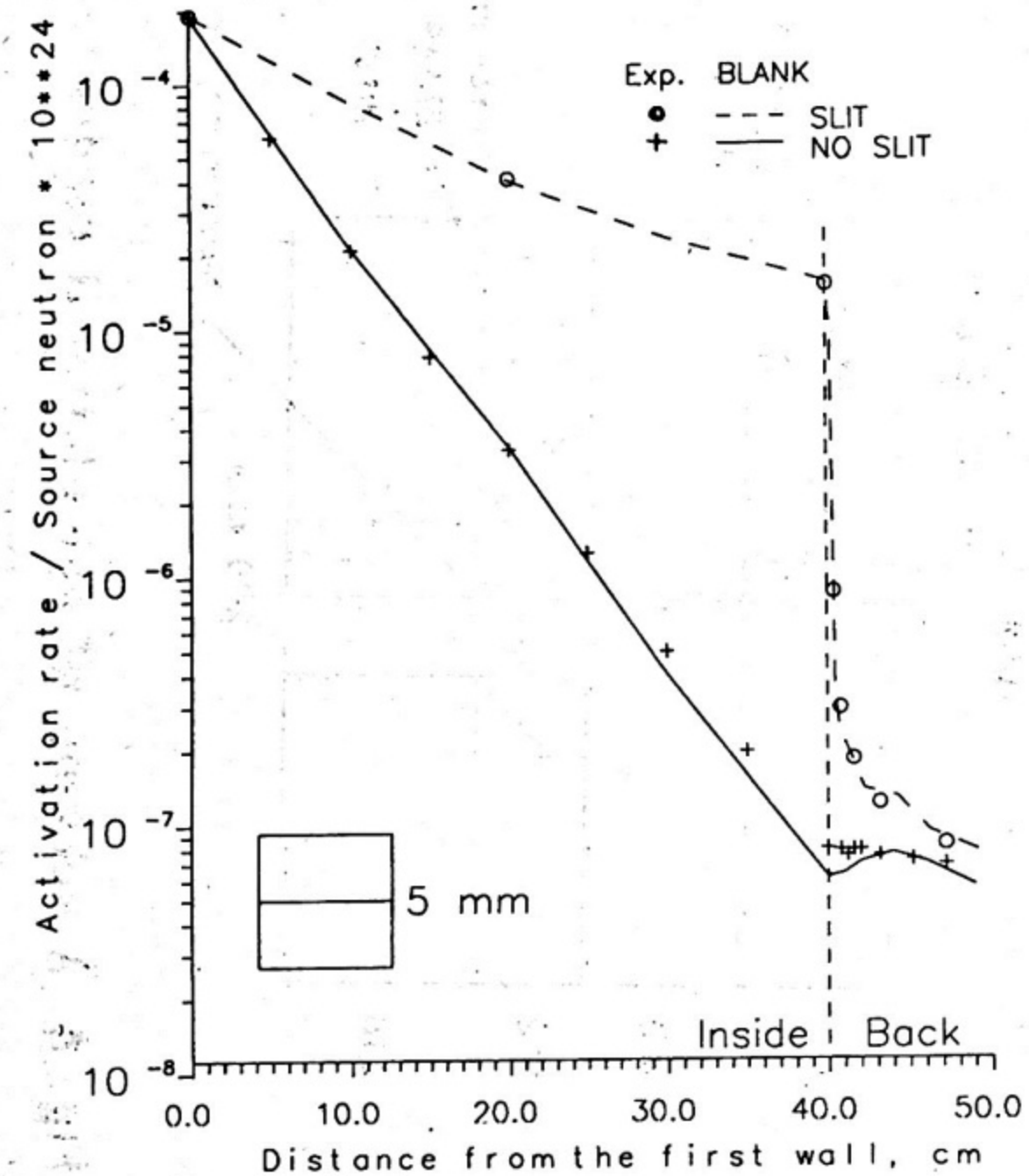

Fig. 6. ^{63}Cu activation rate distribution for a straight slit 5 mm wide.

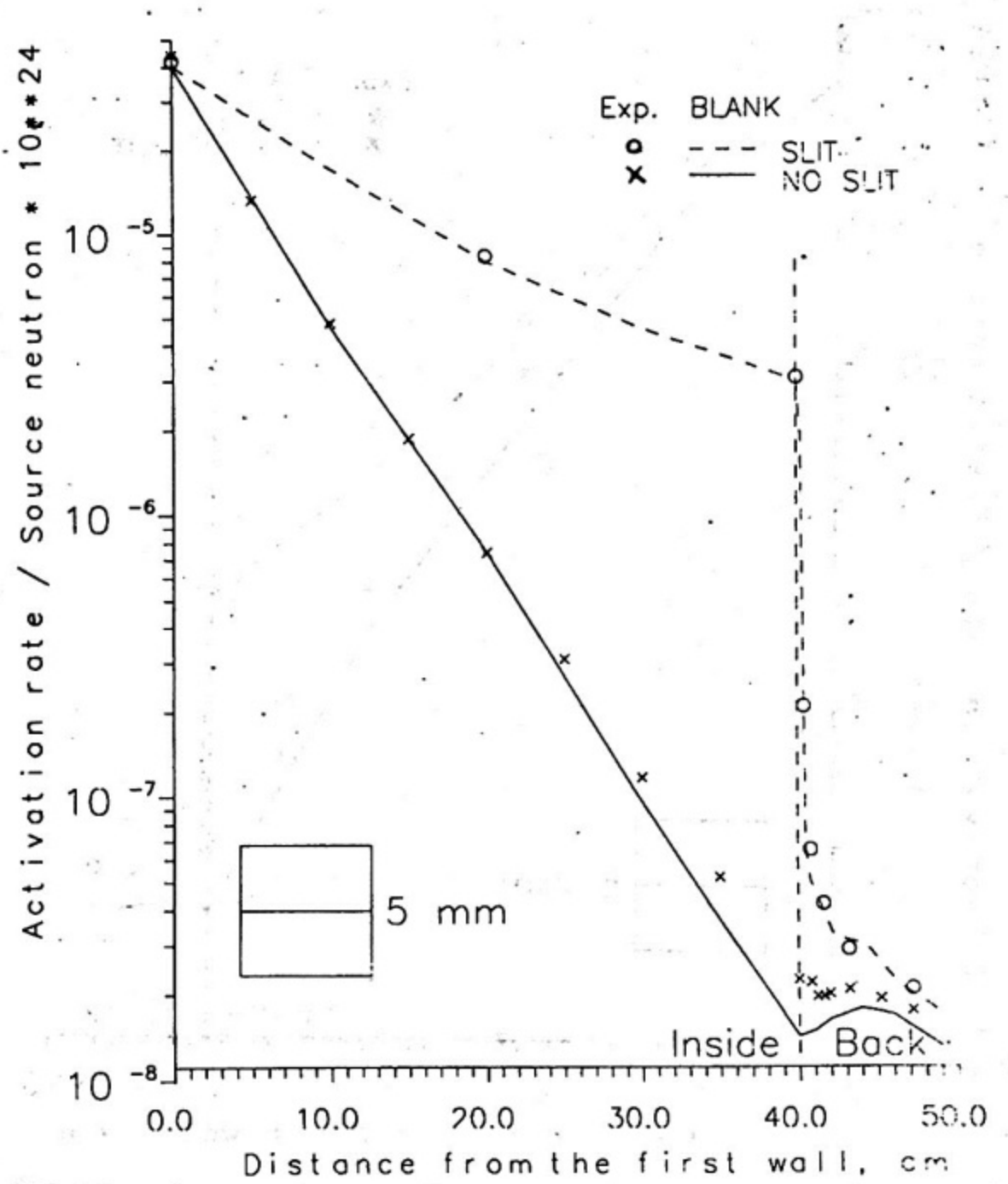

Fig. 7. ^{56}Fe activation rate distribution for a straight slit 5 mm wide.

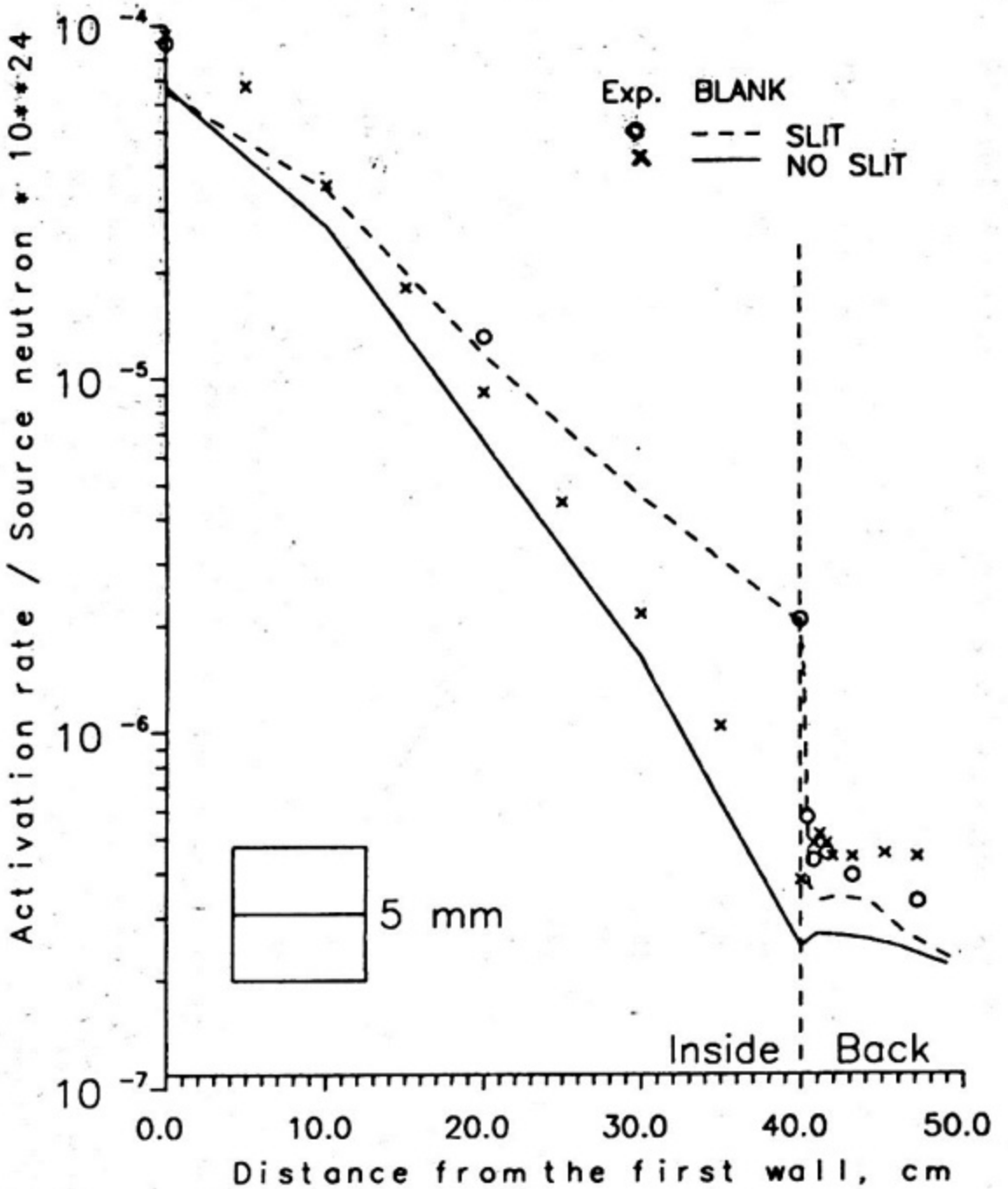

Fig. 8. ^{115}In activation rate distribution for a straight slit 5 mm wide.

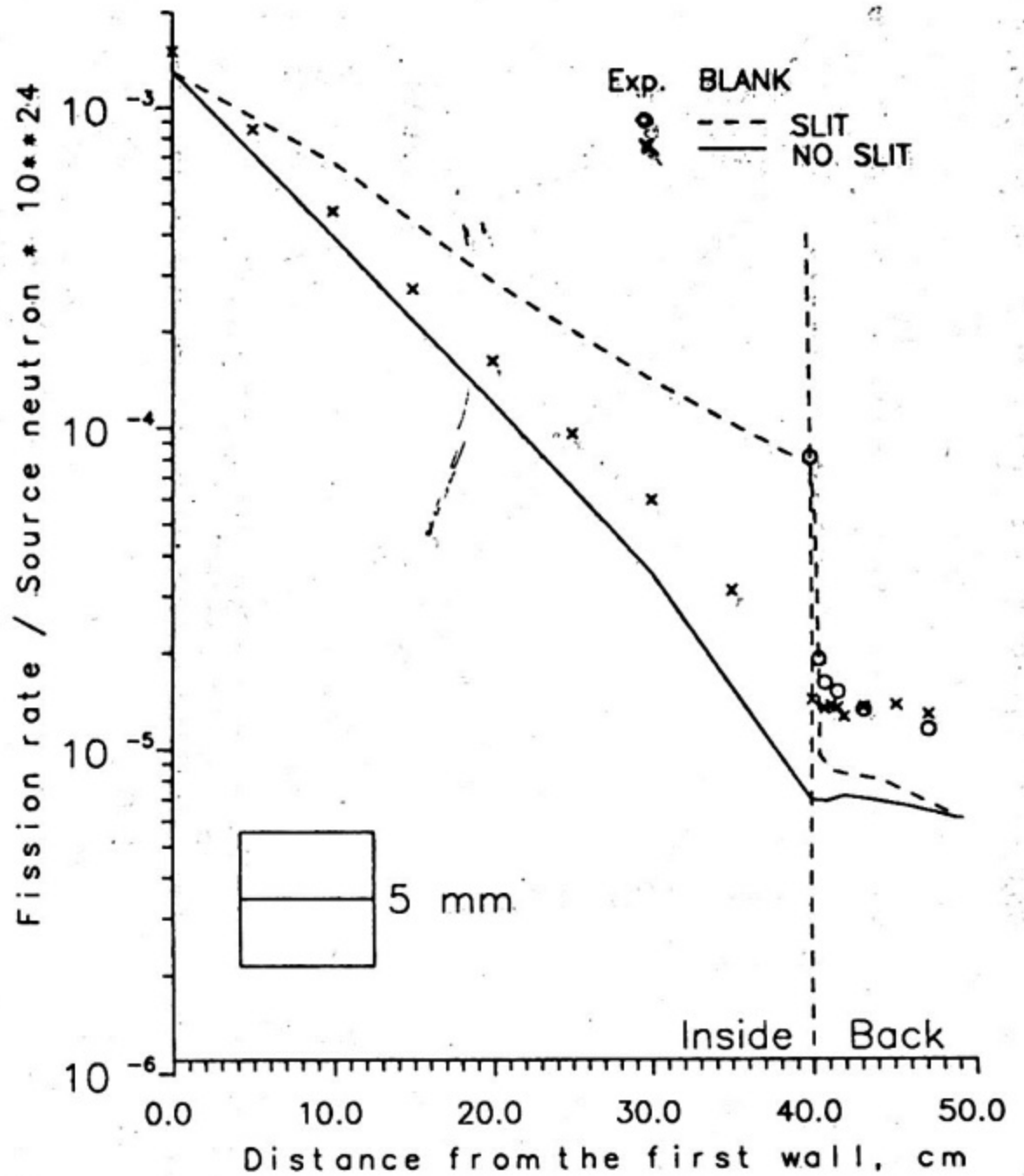

Fig. 9. ^{237}Np fission rate distribution for a straight slit 5 mm wide.

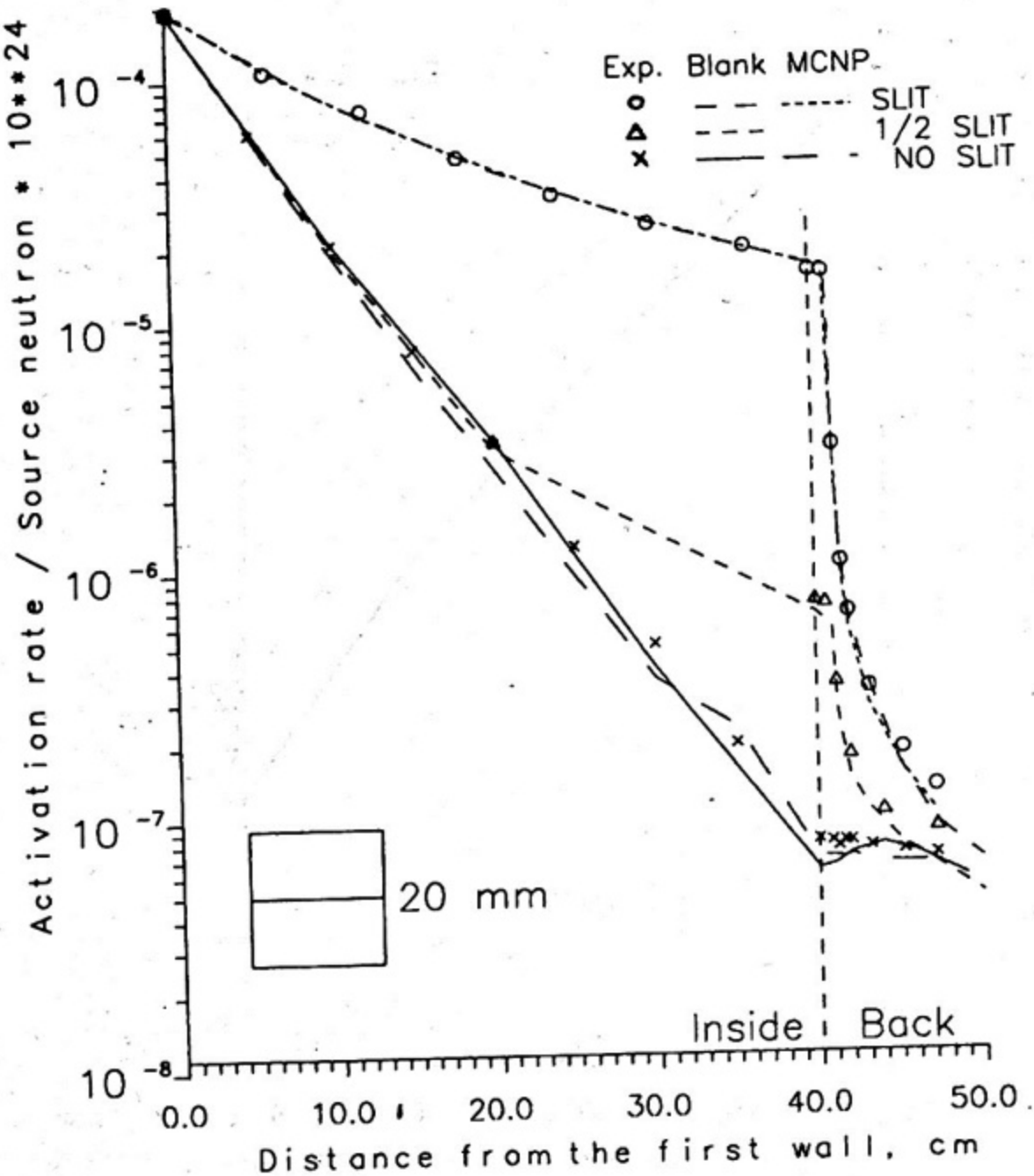

Fig. 10. ^{63}Cu activation rate distribution for a straight slit 20 mm wide.

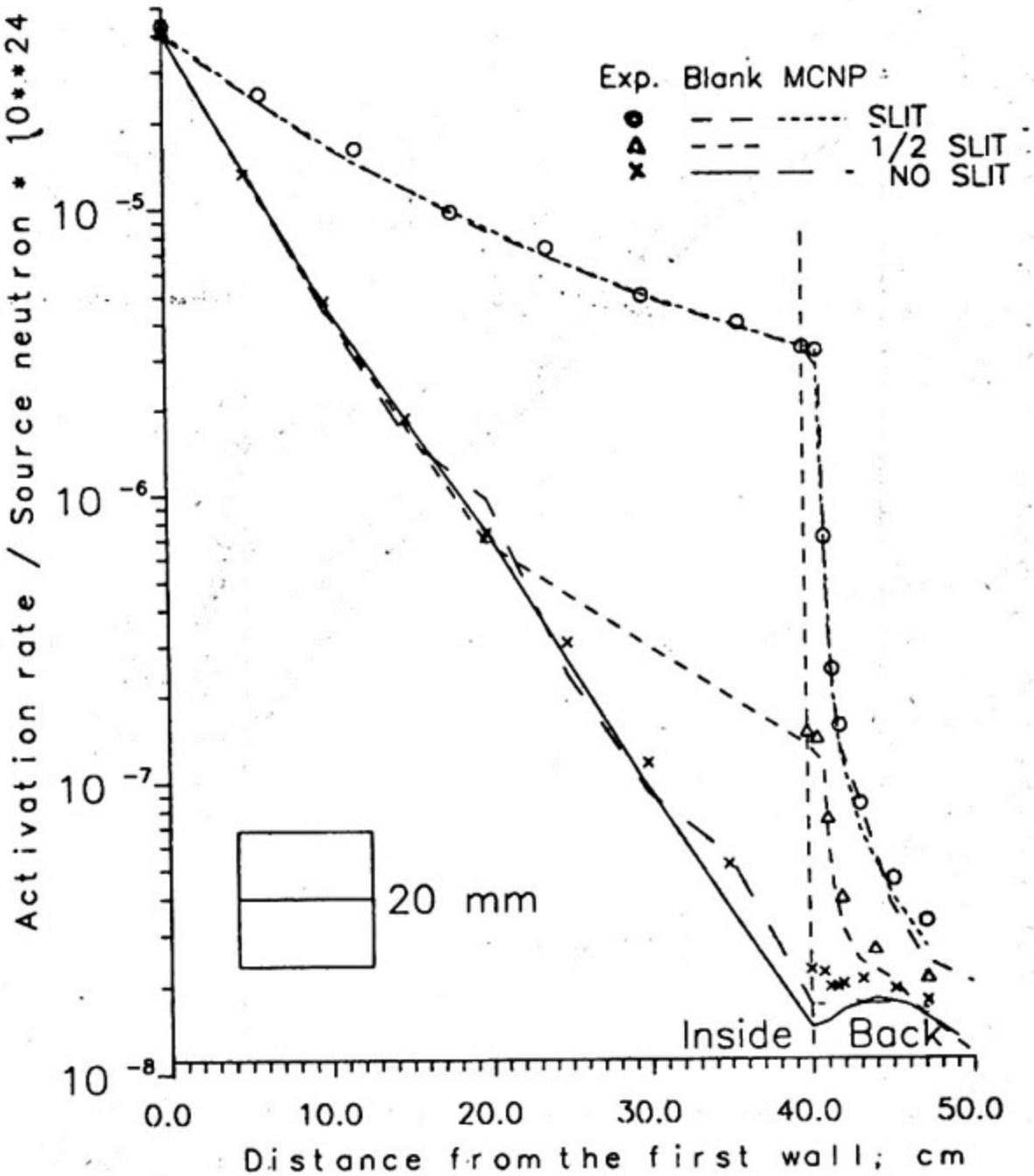

Fig. 11. ^{56}Fe activation rate distribution for a straight slit 20 mm wide.

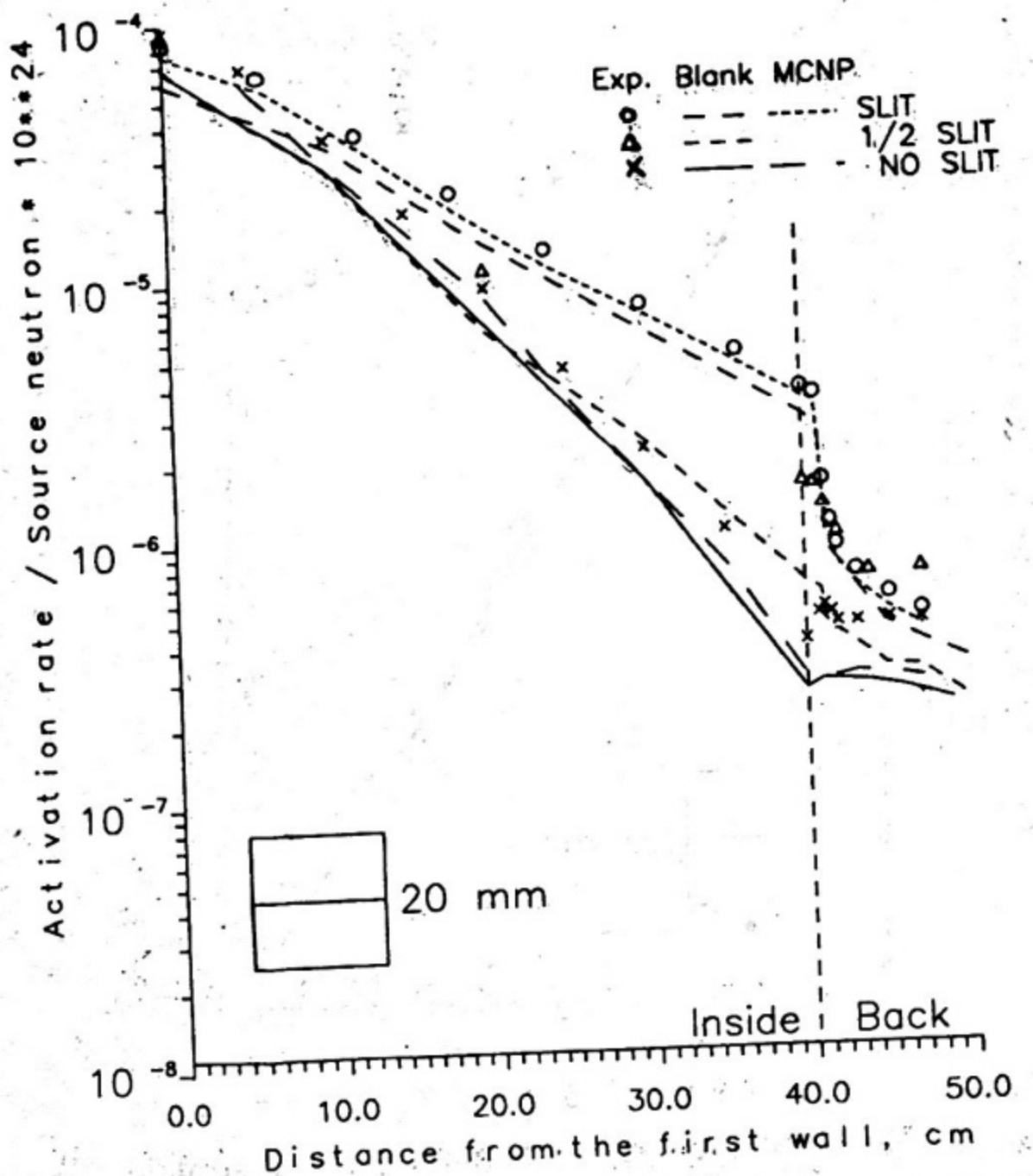

Fig. 12. ^{115}In activation rate distribution for a straight slit 20 mm wide.

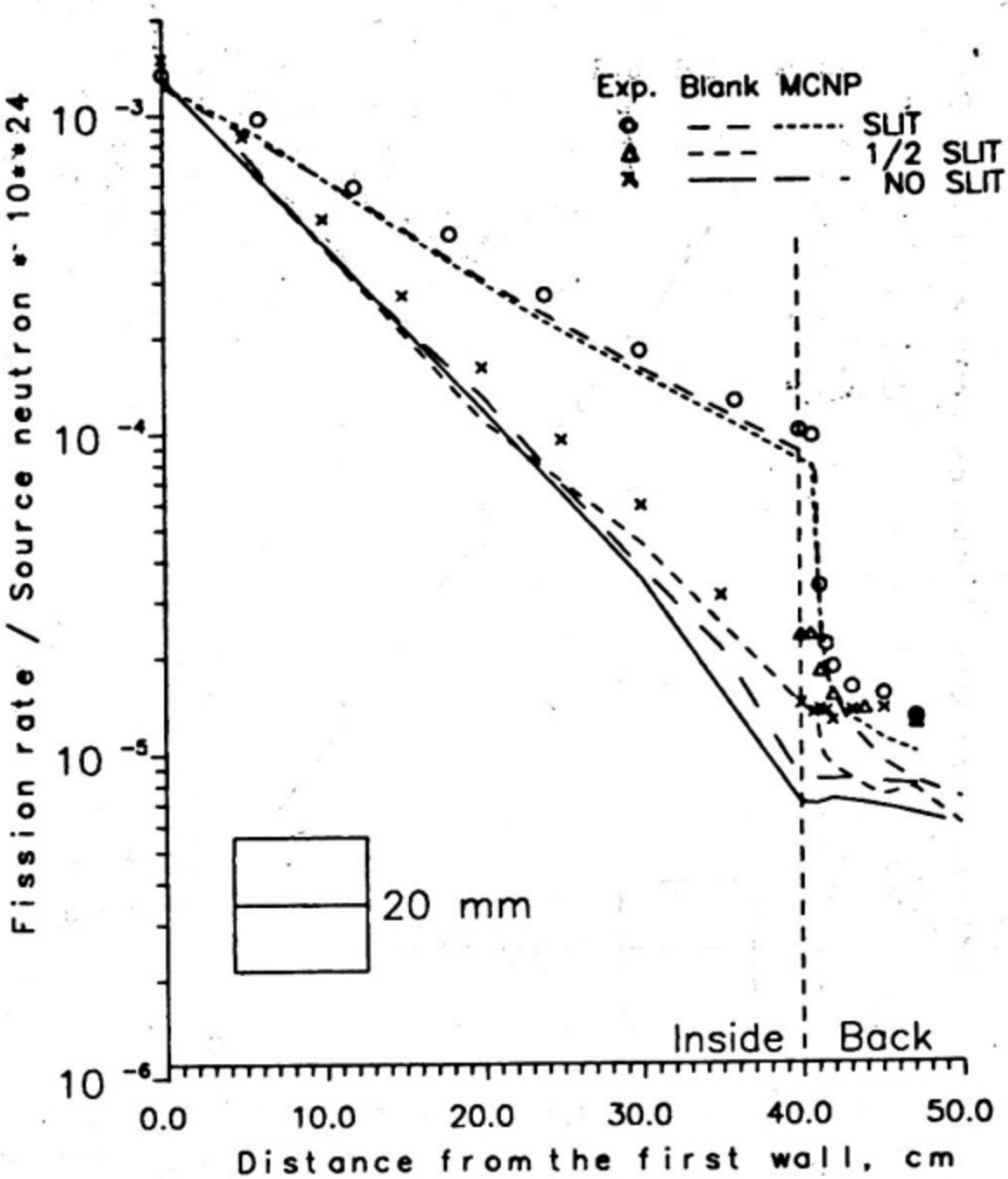

Fig. 13. ^{237}Np fission rate distribution for a straight slit 20 mm wide.

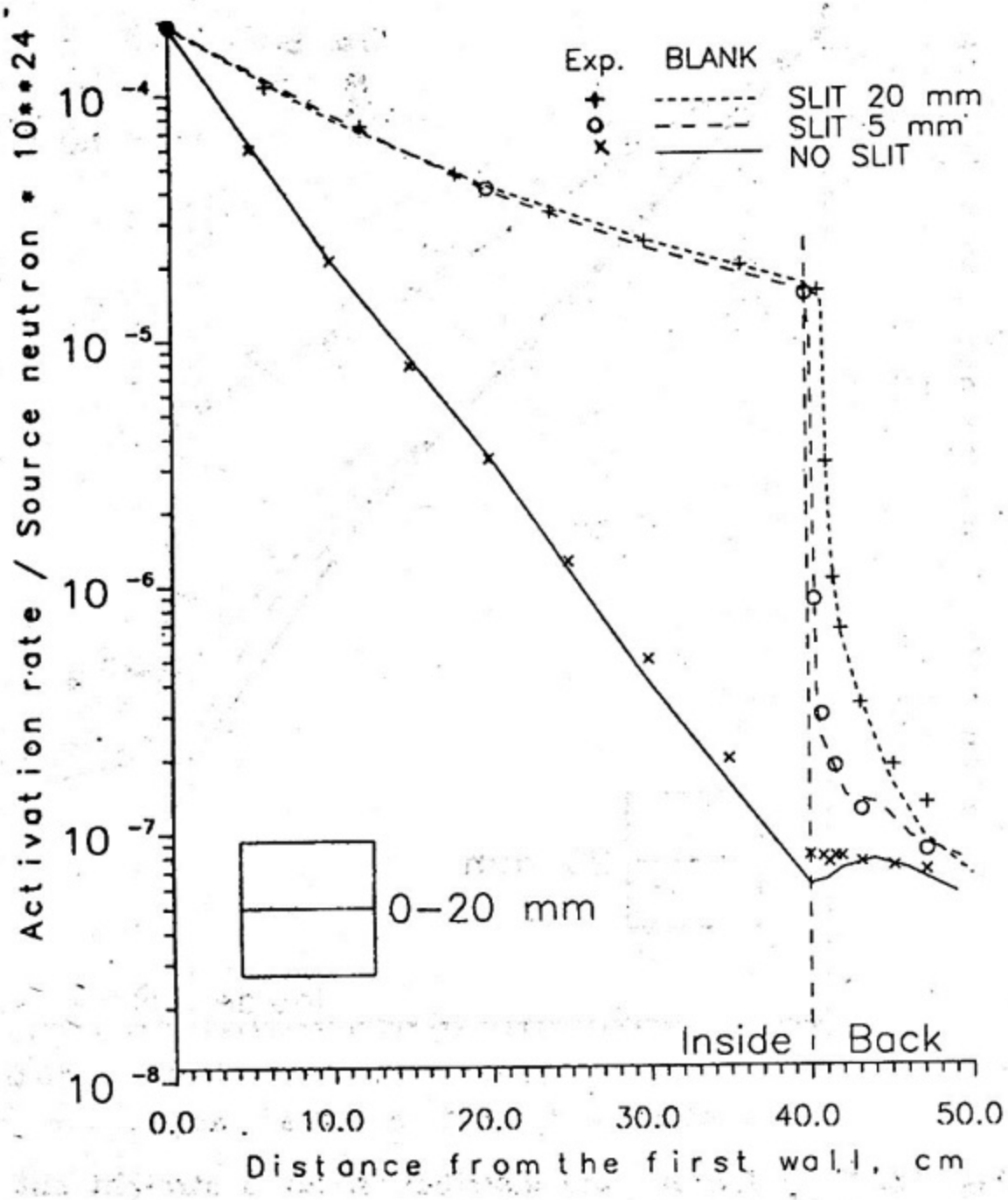

Fig. 14. ^{63}Cu activation rate distributions for different widths of a straight slit.

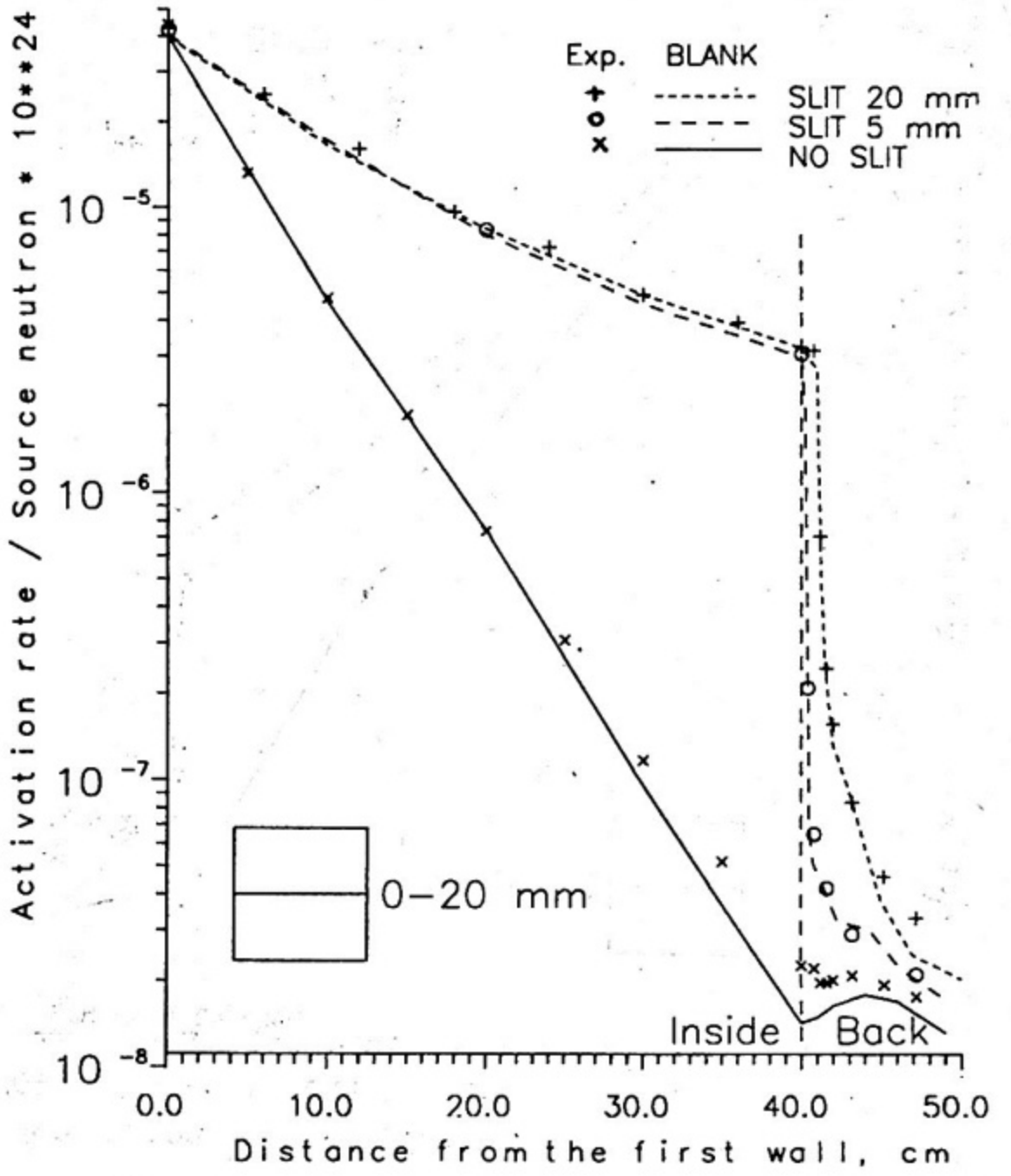

Fig. 15. ^{56}Fe activation rate distributions for different widths of a straight slit.

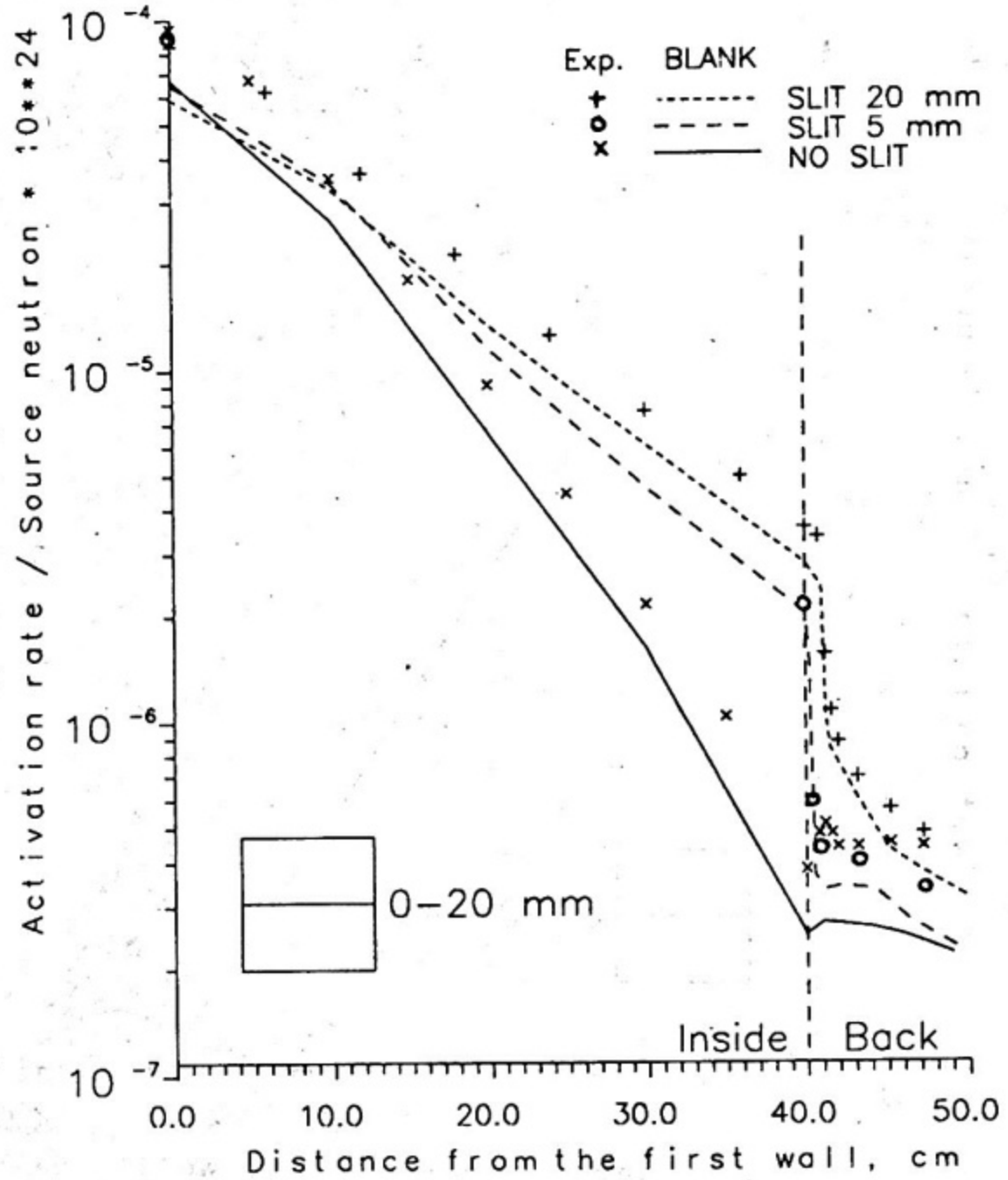

Fig. 16. ^{115}In activation rate distributions for different widths of a straight slit.

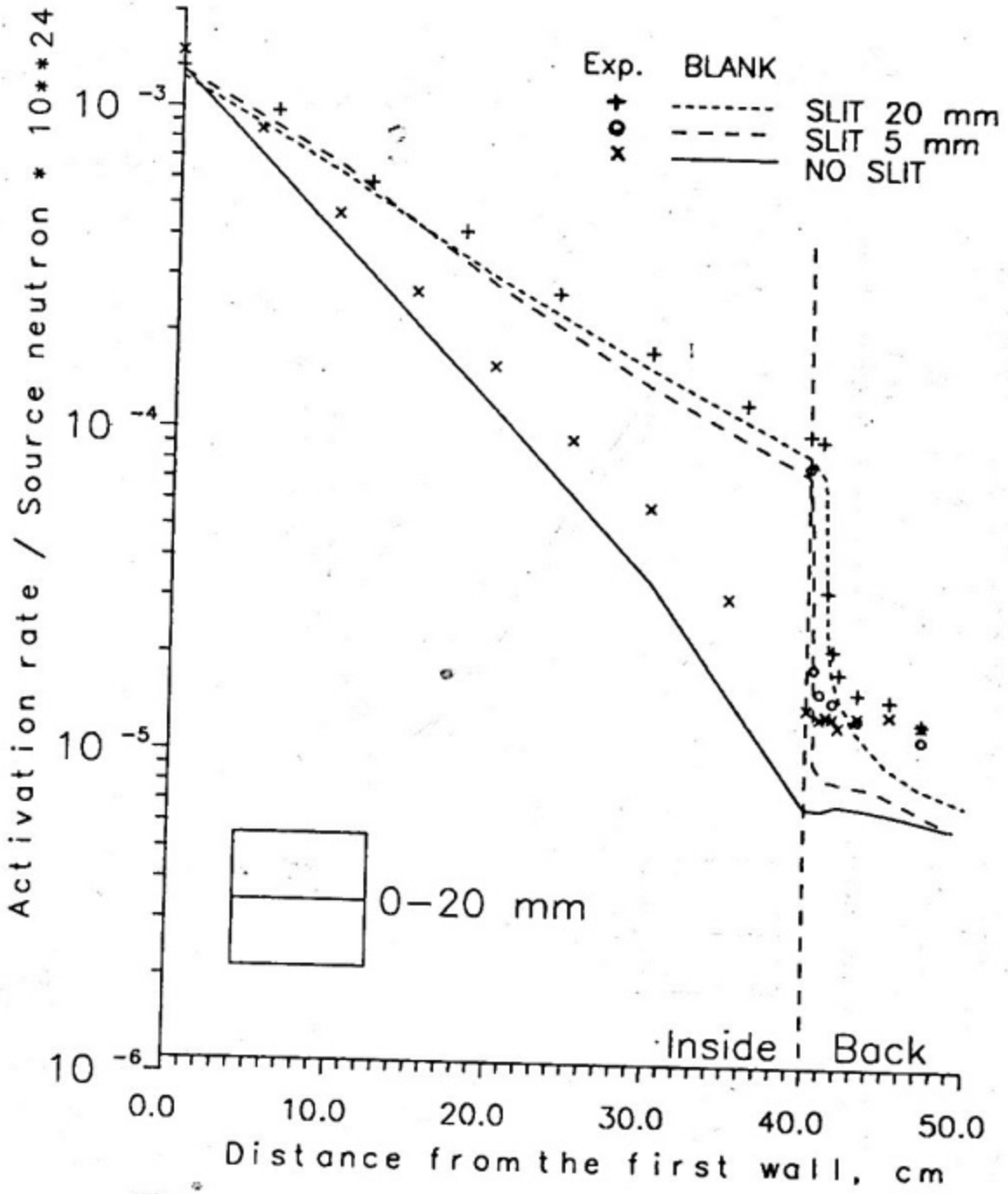

Fig. 17. ^{237}Np activation rate distributions for different widths of a straight slit.

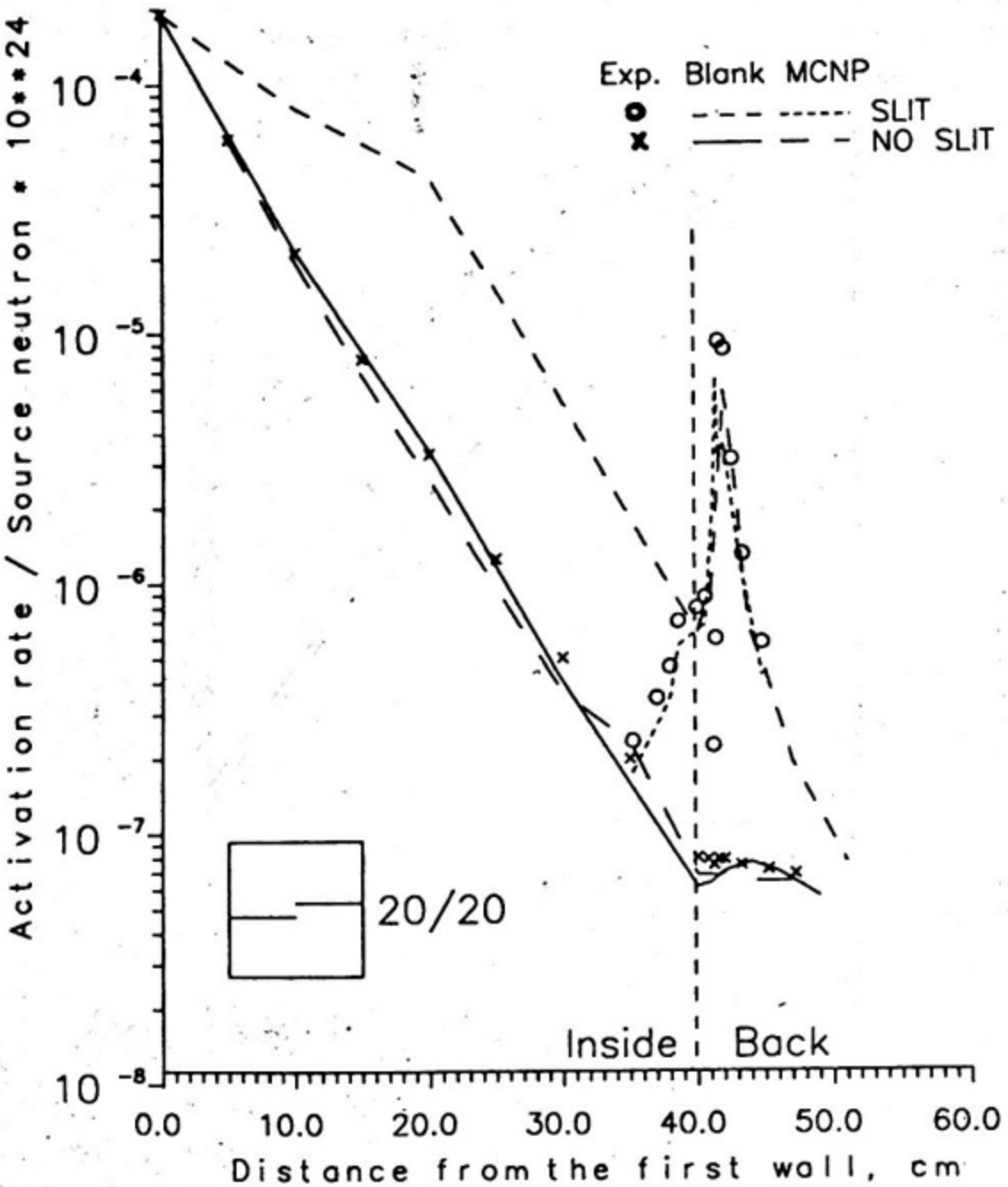

Fig. 18. ^{63}Cu activation rate distribution for a slit 20 mm wide shifted on 20 mm.

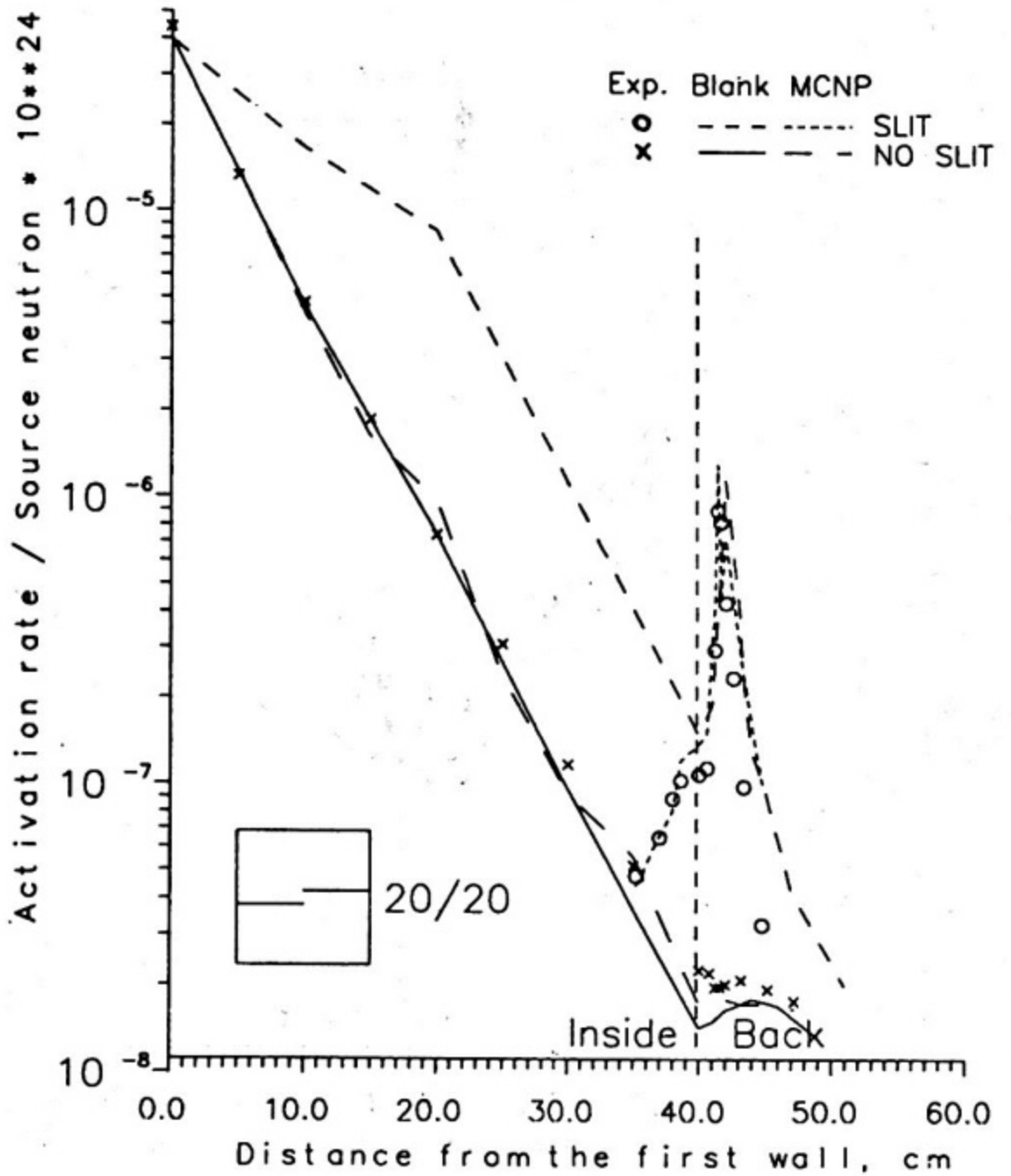

Fig. 19. ^{56}Fe activation rate distribution for a slit 20 mm wide shifted on 20 mm.

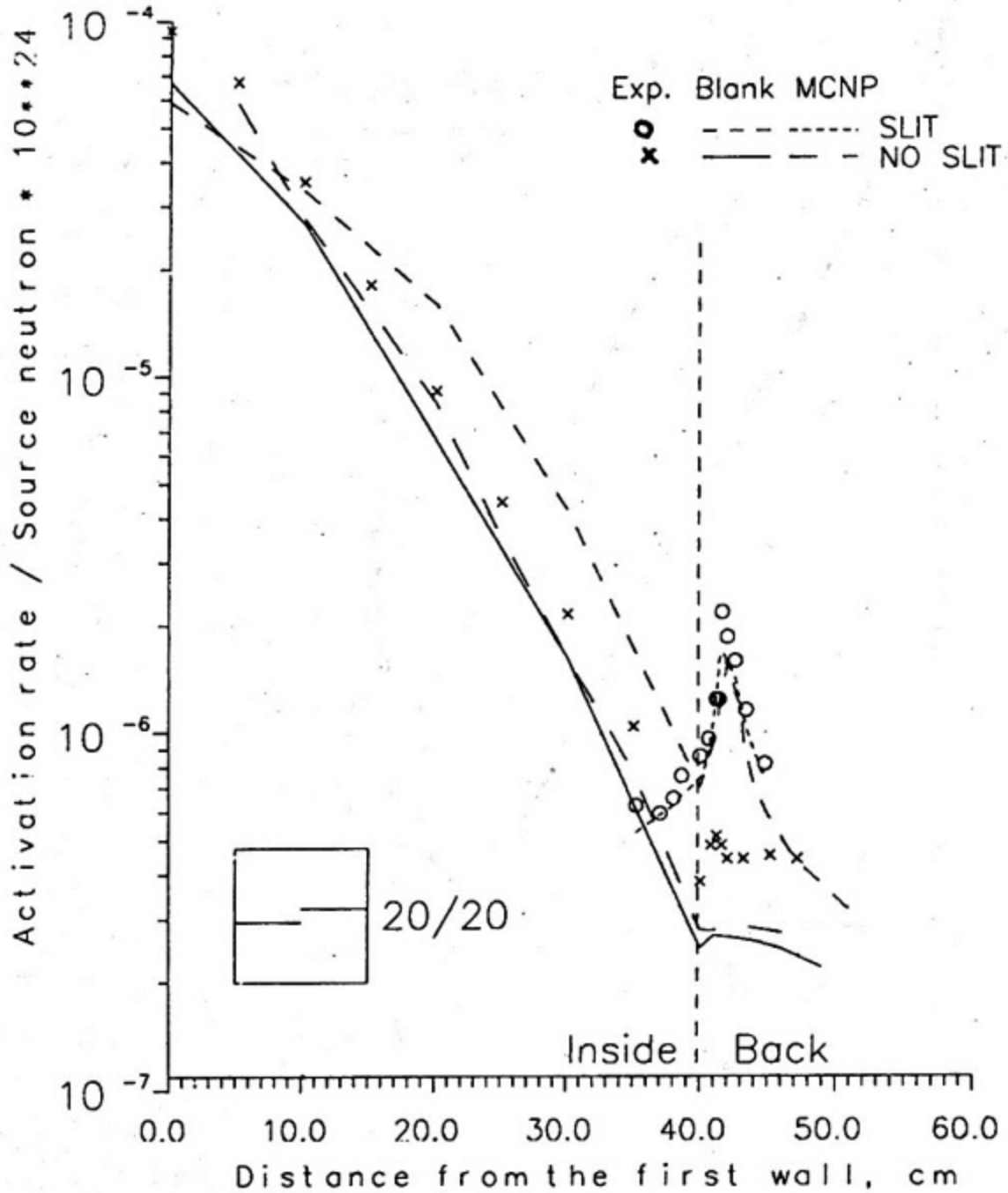

Fig. 20. ^{115}In activation rate distribution for a slit 20 mm wide shifted by 20 mm.

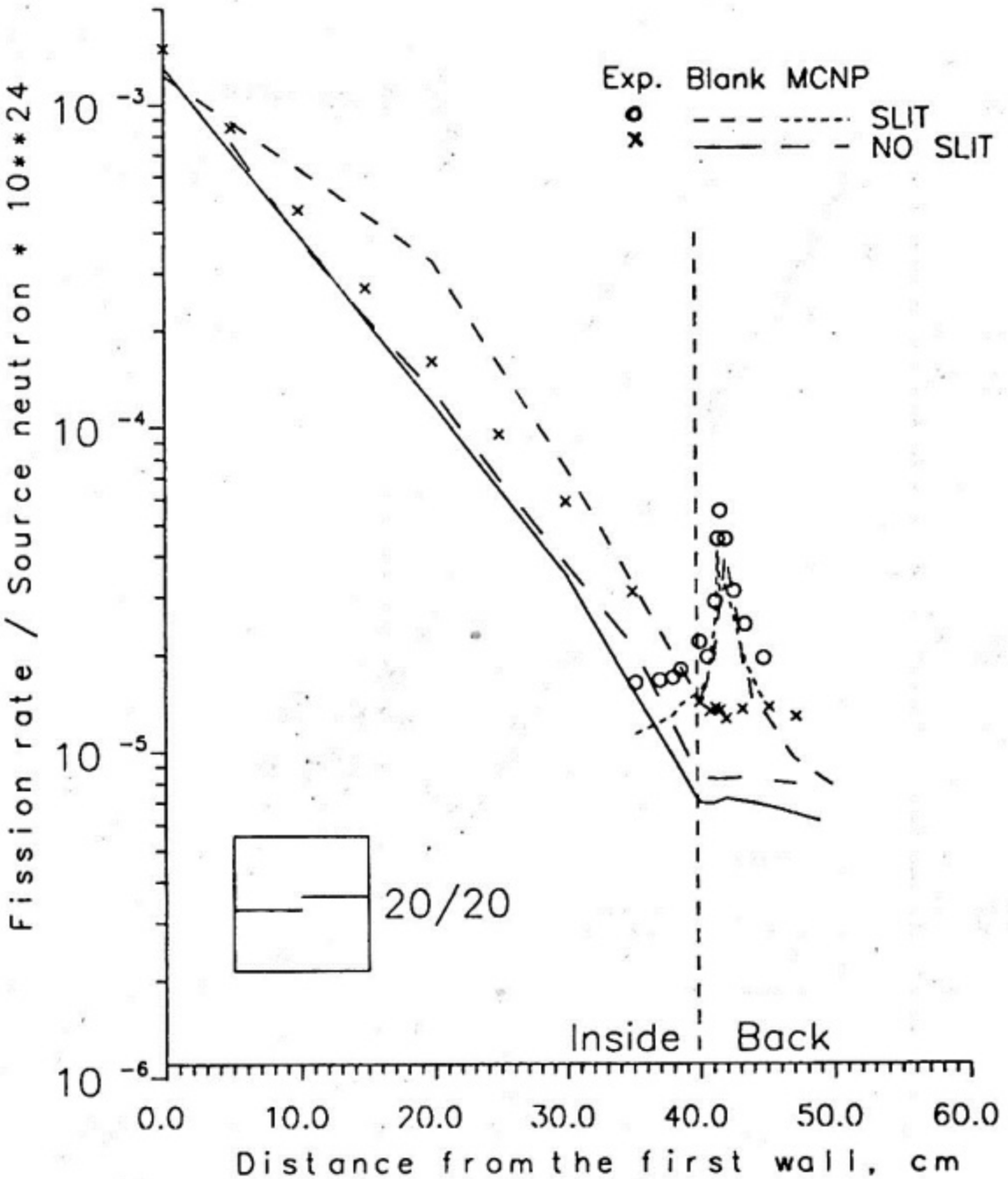

Fig. 21. ^{237}Np fission rate distribution for a slit 20 mm wide shifted on 20 mm.

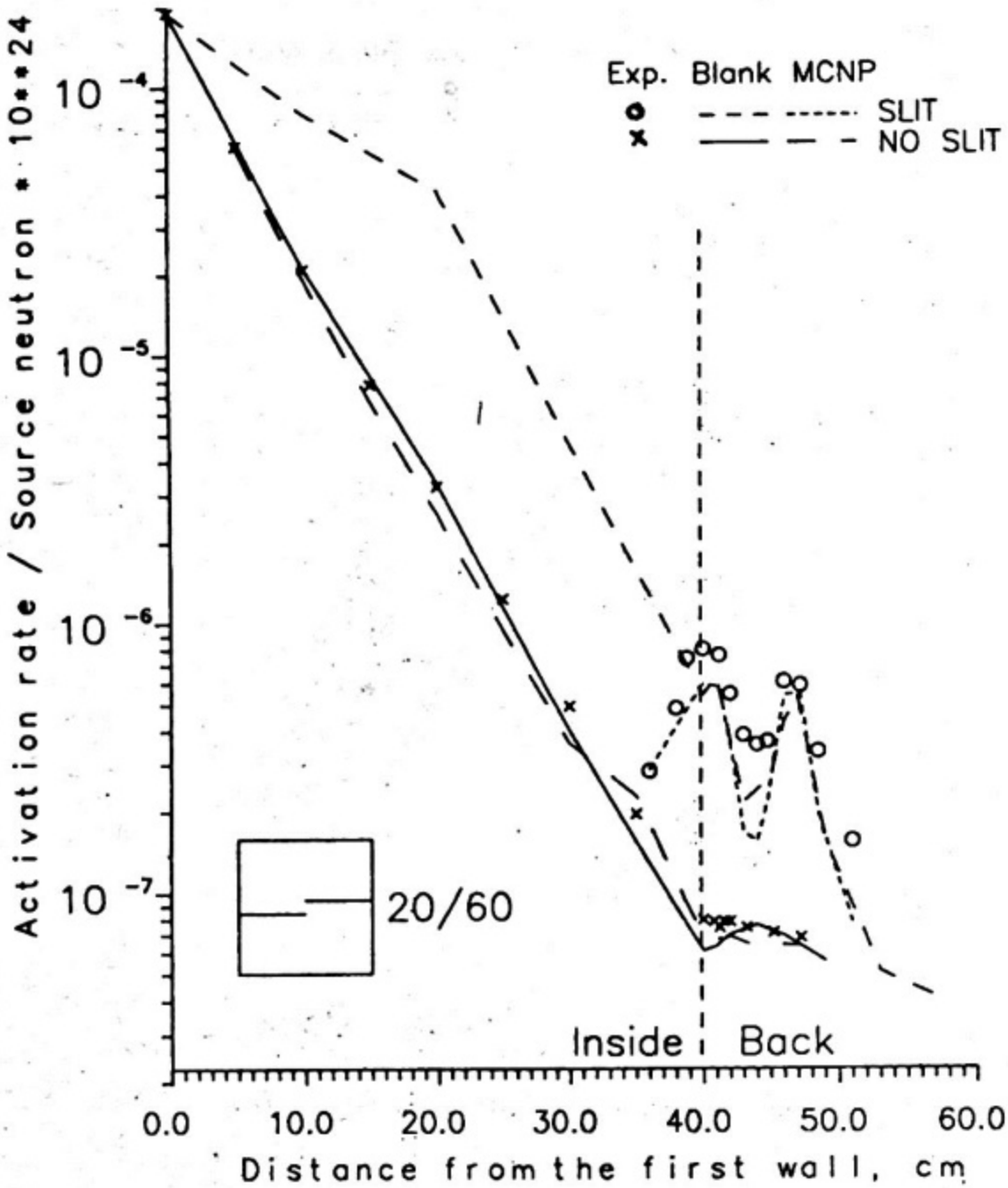

Fig. 22. ^{63}Cu activation rate distribution for a slit 20 mm wide shifted on 60 mm.

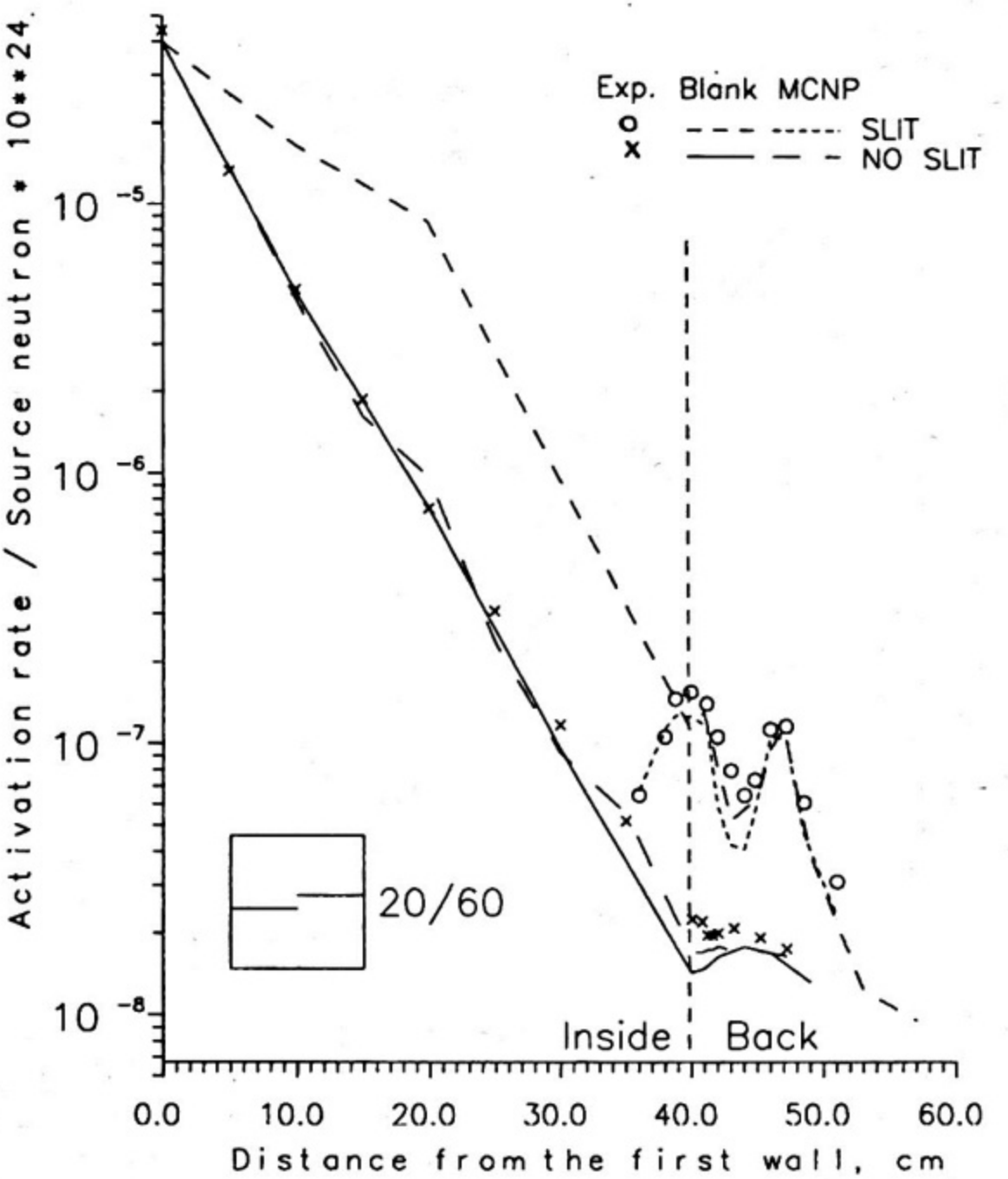

Fig. 23. ^{56}Fe activation rate distribution for a slit 20 mm wide shifted on 60 mm.

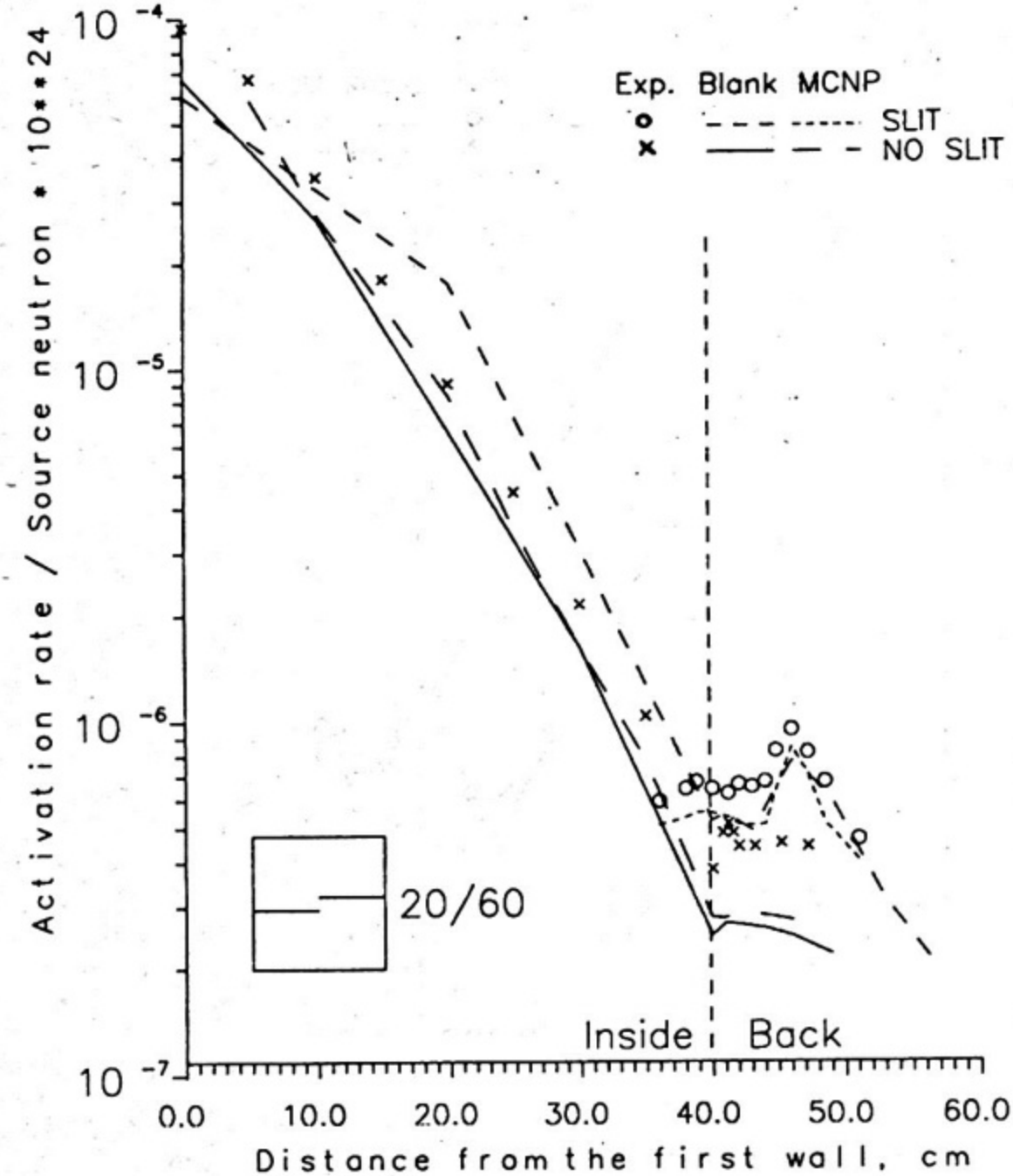

Fig. 24. ^{115}In activation rate distribution for a slit 20 mm wide shifted on 60 mm.

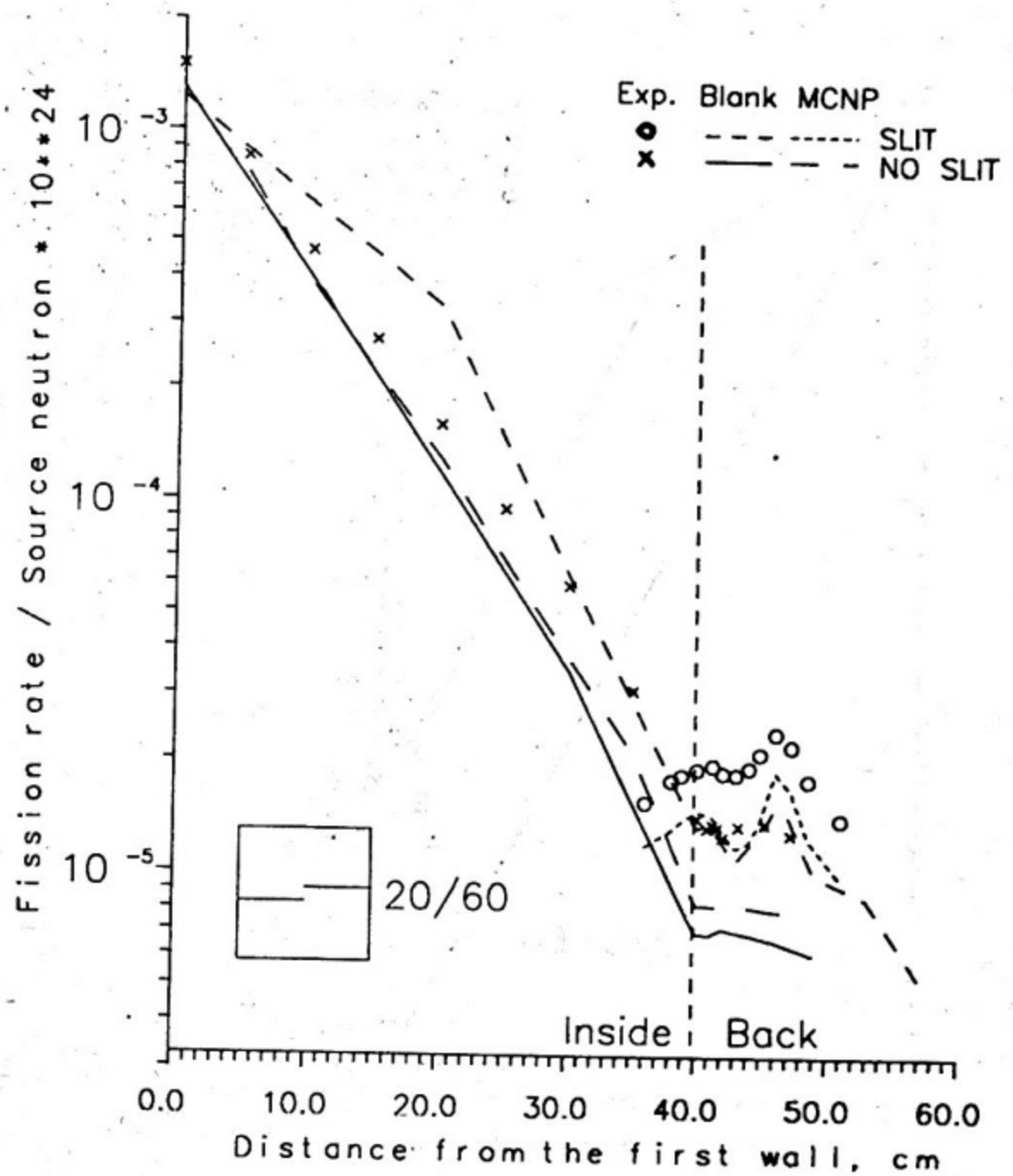

Fig. 25. ^{237}Np fission rate distribution for a slit 20 mm wide shifted on 60 mm.

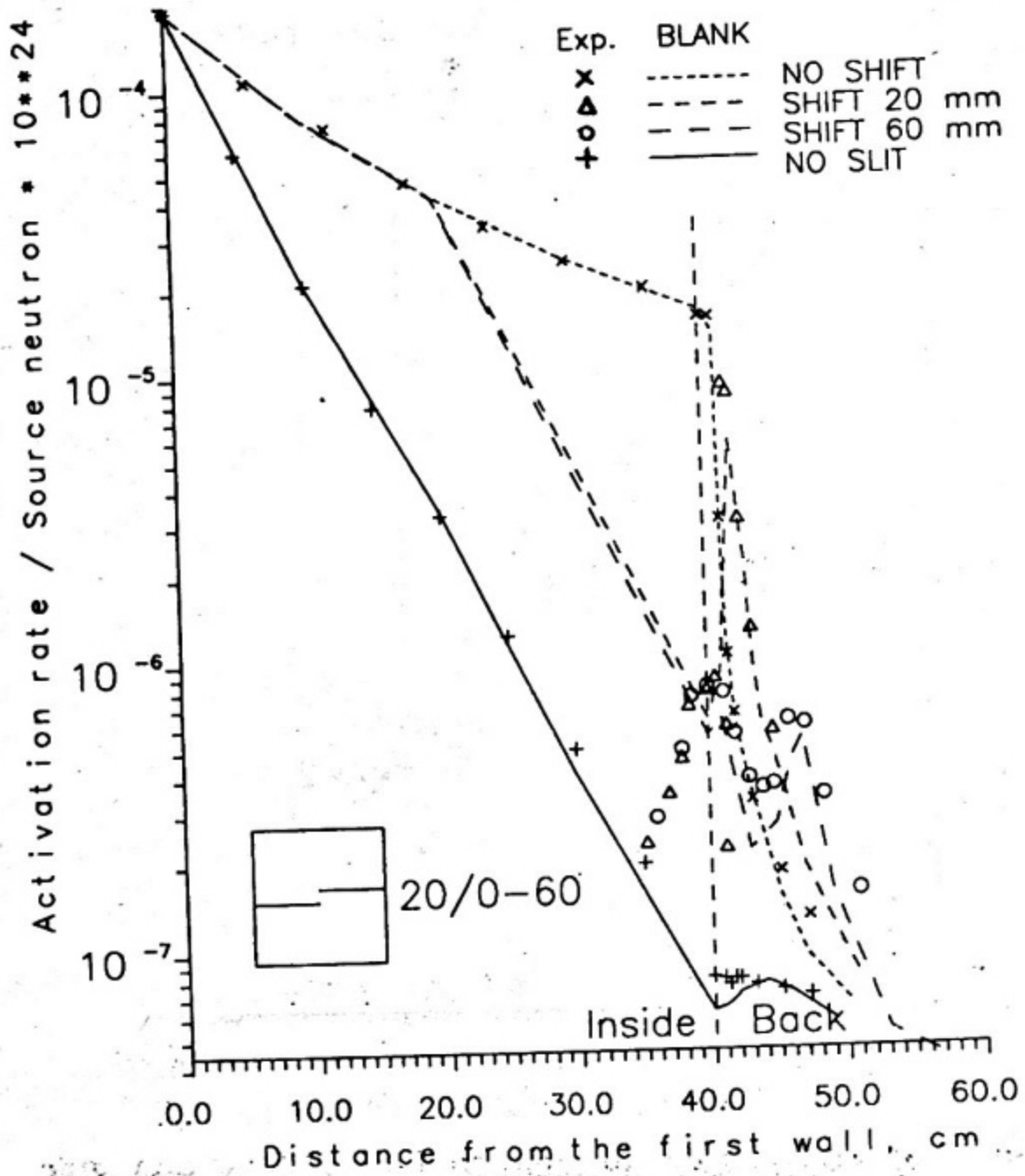

Fig. 26. ^{63}Cu activation rate distributions for a slit 20 mm wide and different shift values.

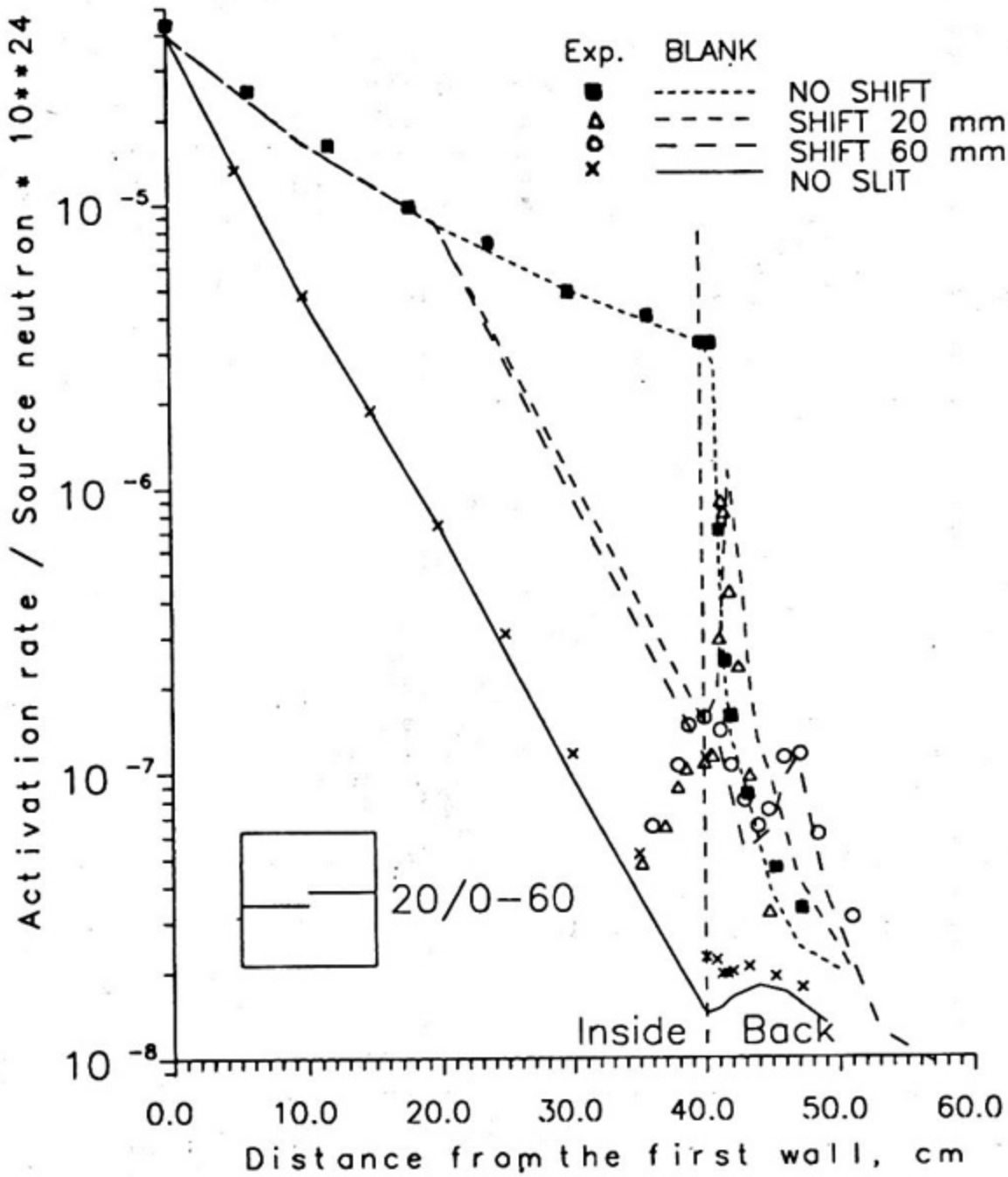

Fig. 27. ^{56}Fe activation rate distributions for a slit 20 mm wide and different shift values.

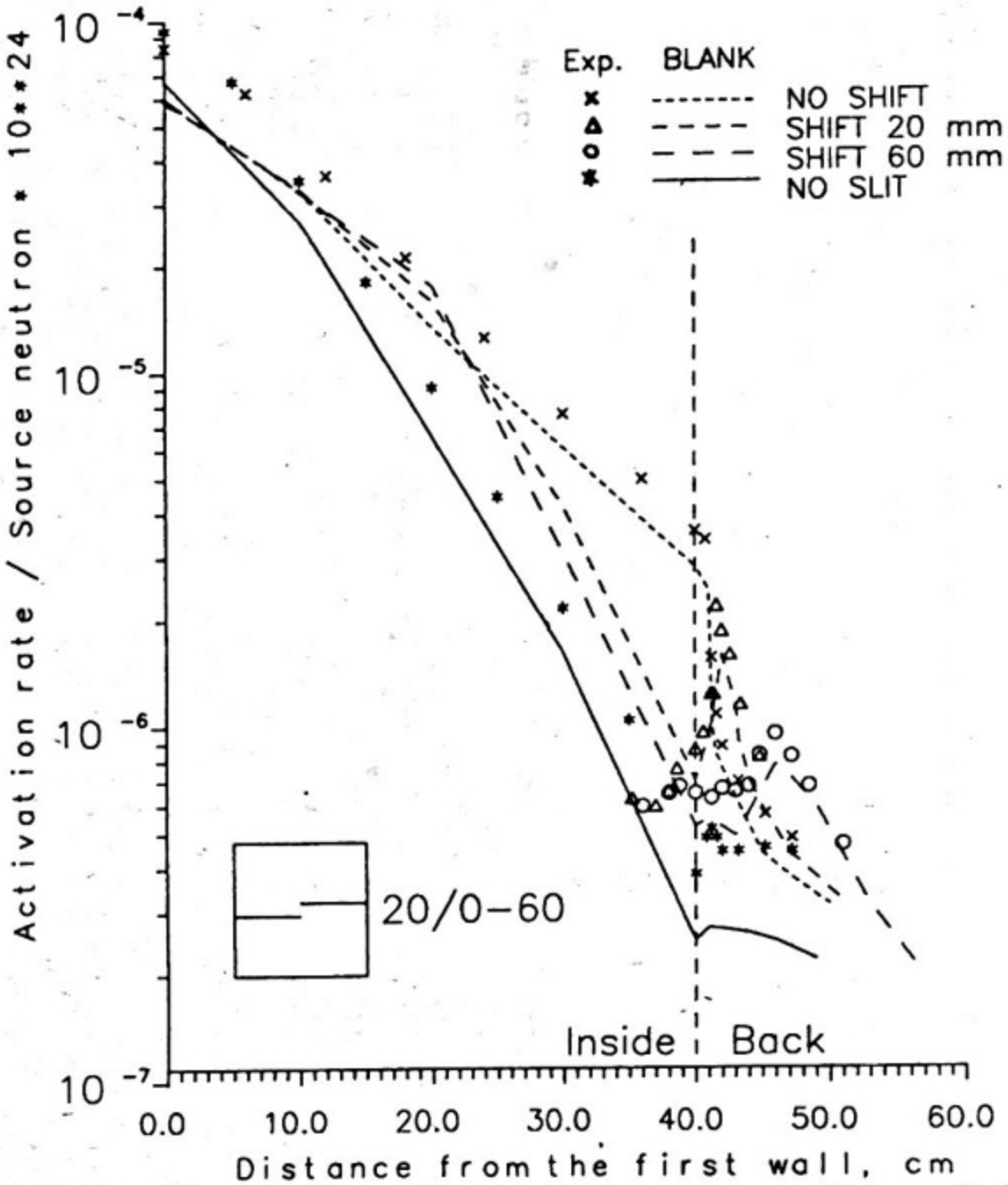

Fig. 28. ^{115}In activation rate distributions for a slit 20 mm wide and different shift values.

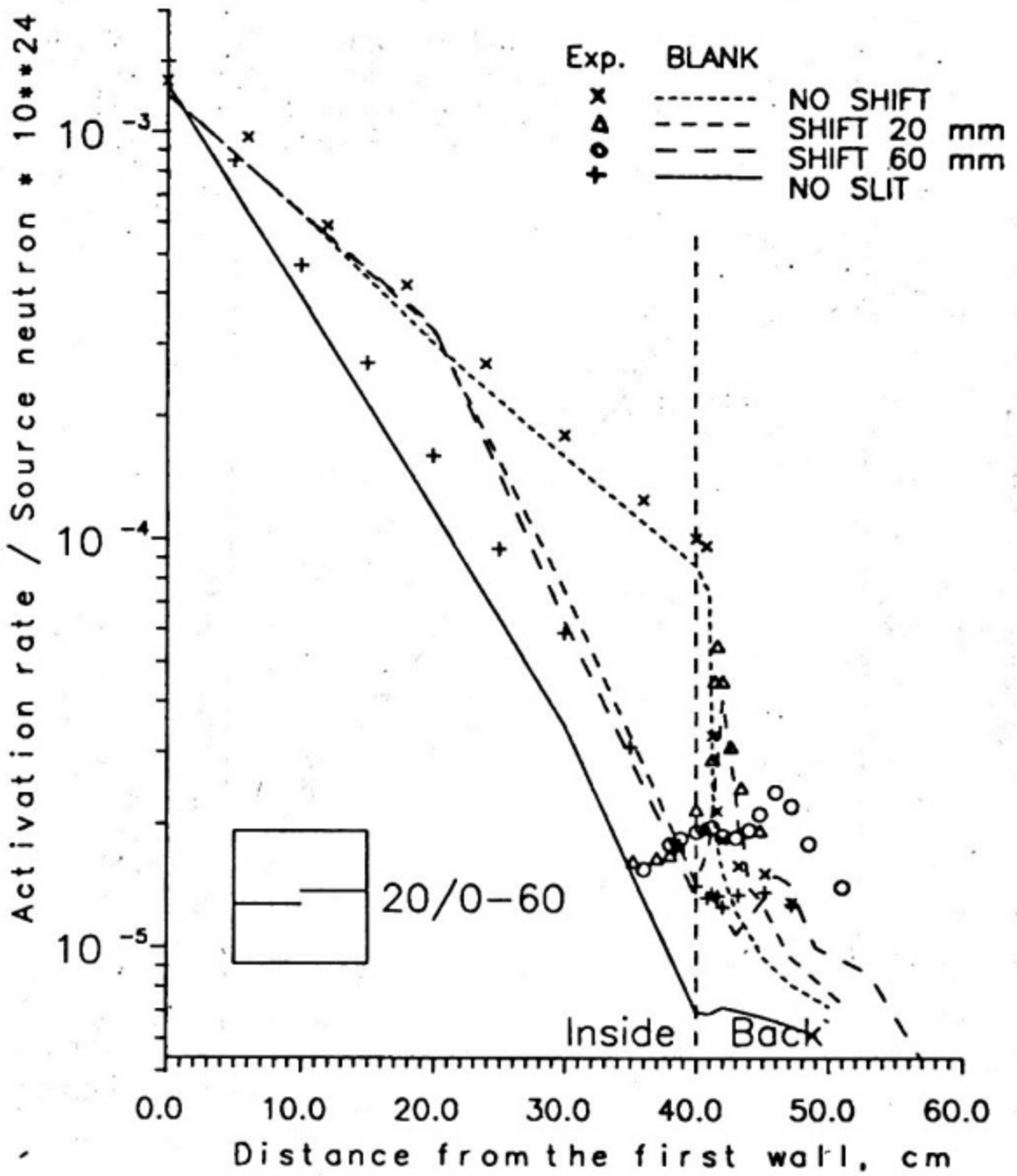

Fig. 29. ^{237}Np activation rate distributions for a slit 20 mm wide and different shift values.

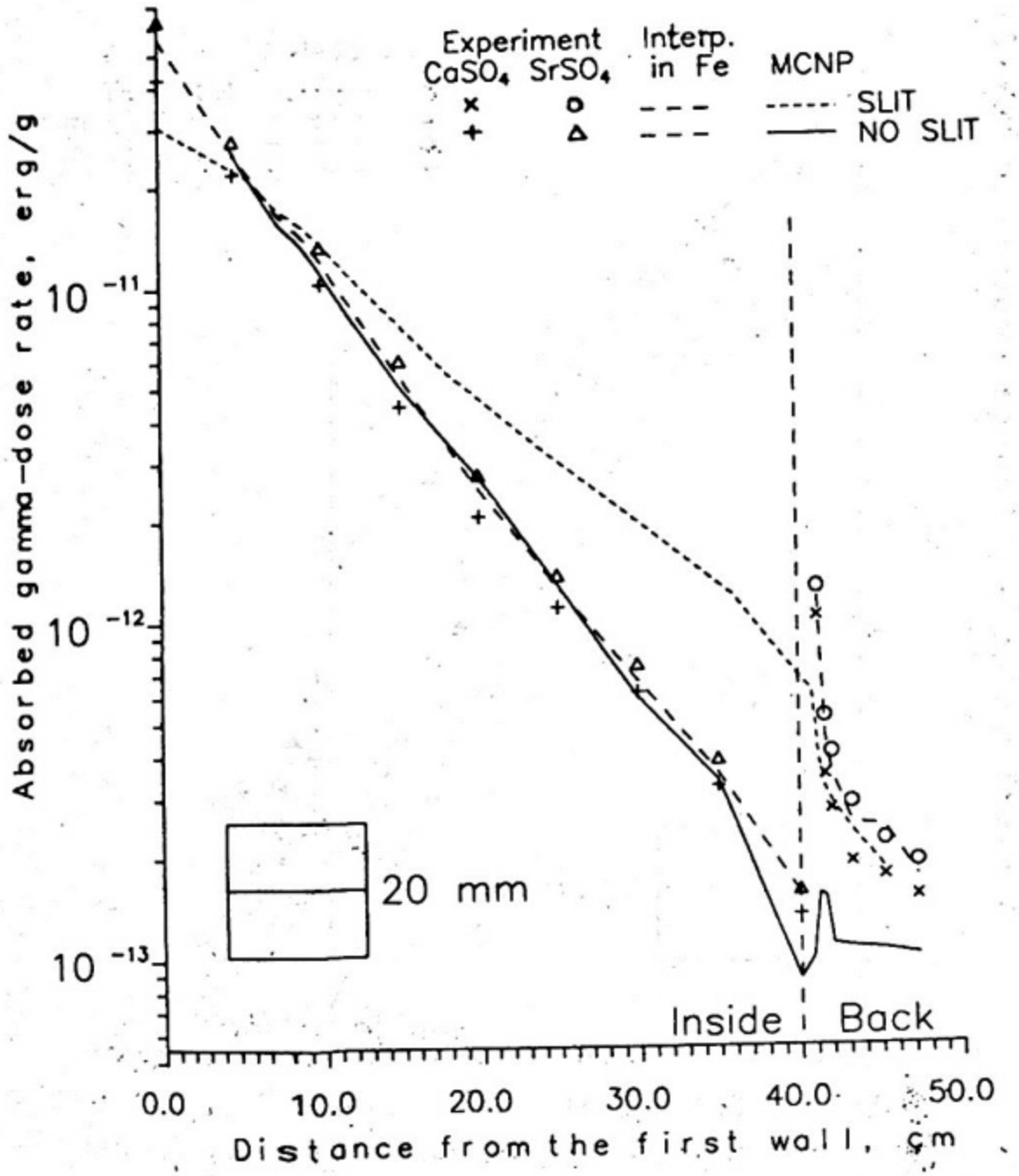

Fig. 30. Gamma-heating rate distribution in iron shield with a straight slit 20 mm wide.

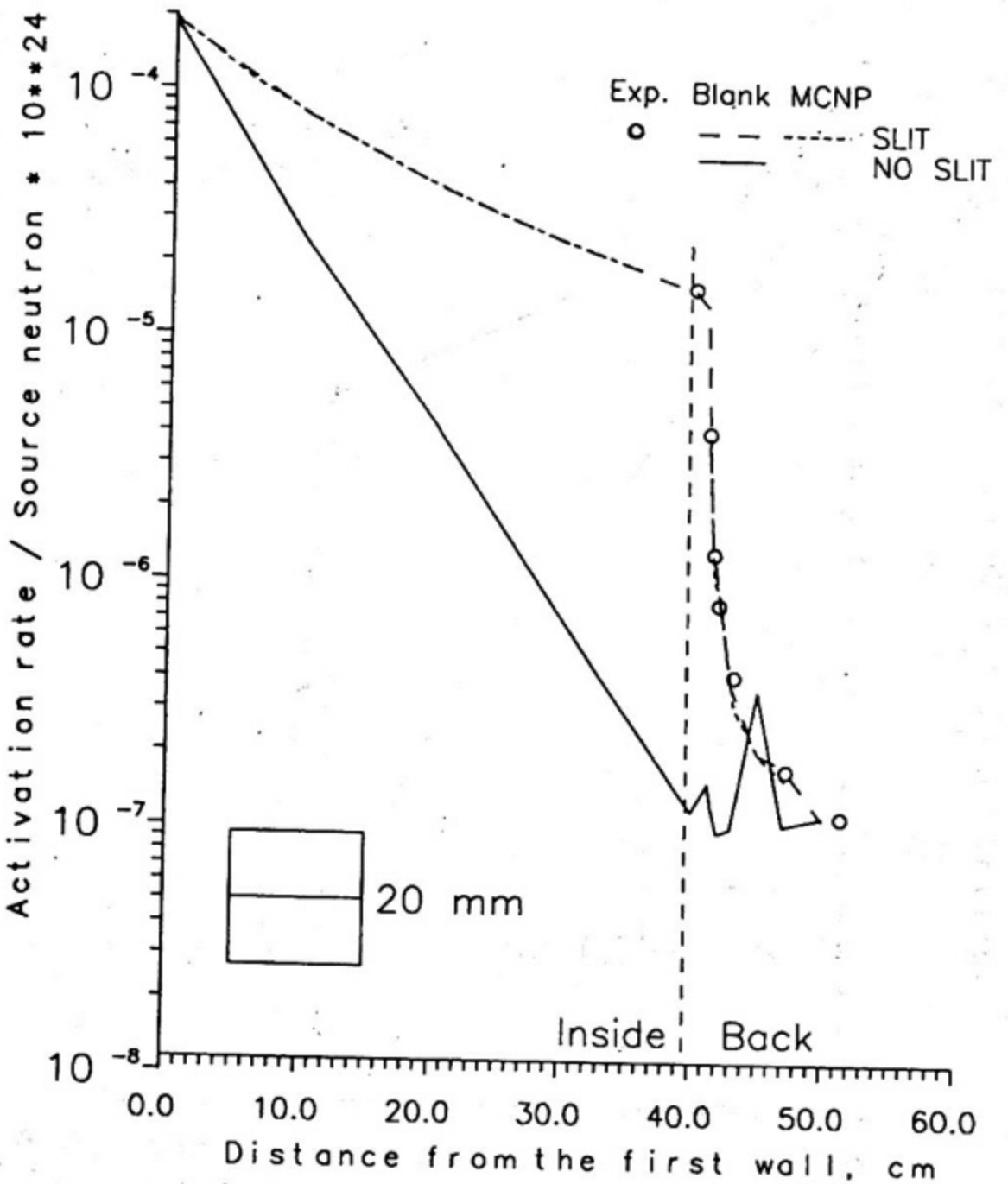

Fig. 31. ^{63}Cu activation rate distribution in the iron–water assembly with a straight slit 20 mm wide.

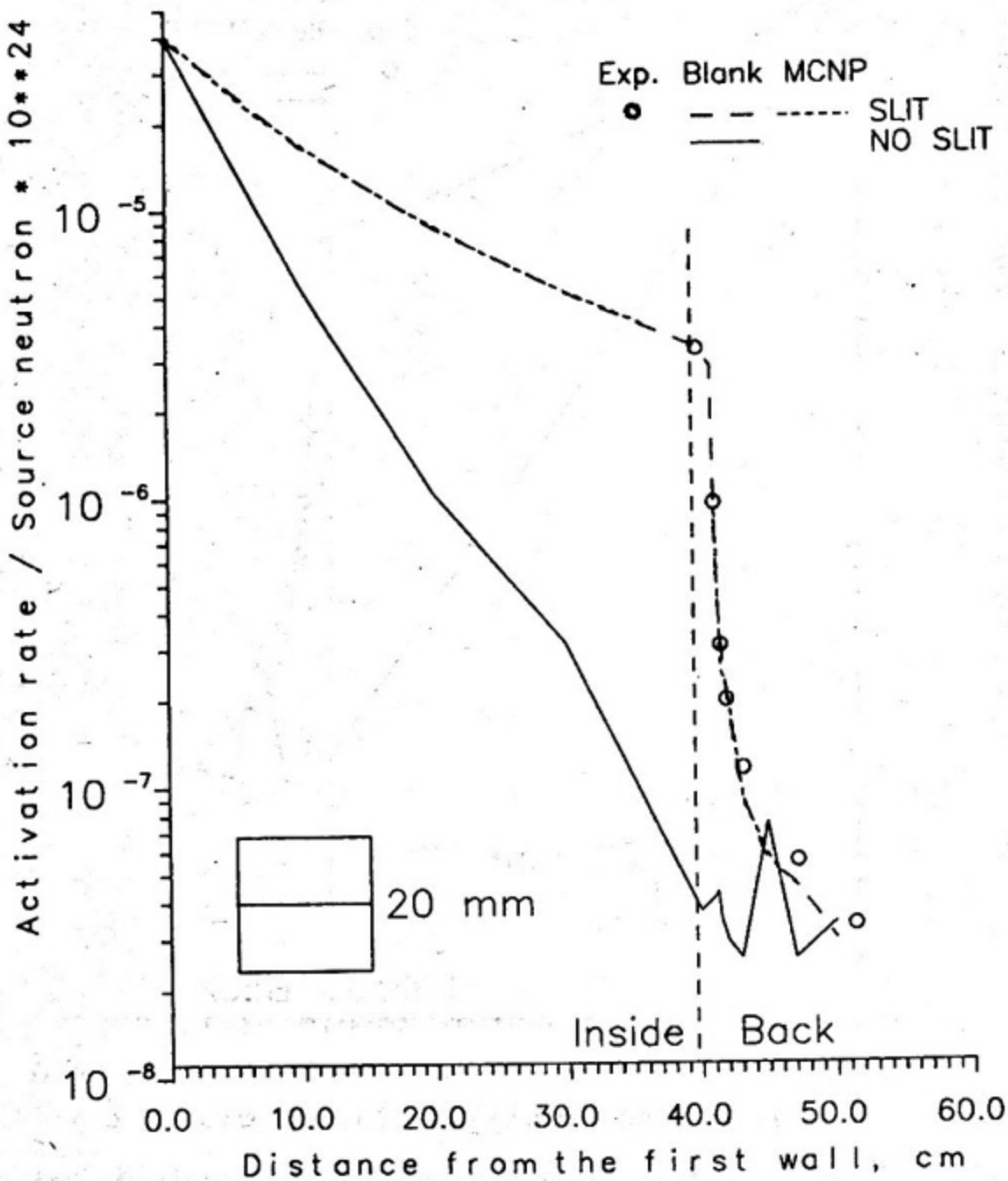

Fig. 32. ^{56}Fe activation rate distribution in the iron–water assembly with a straight slit 20 mm wide.

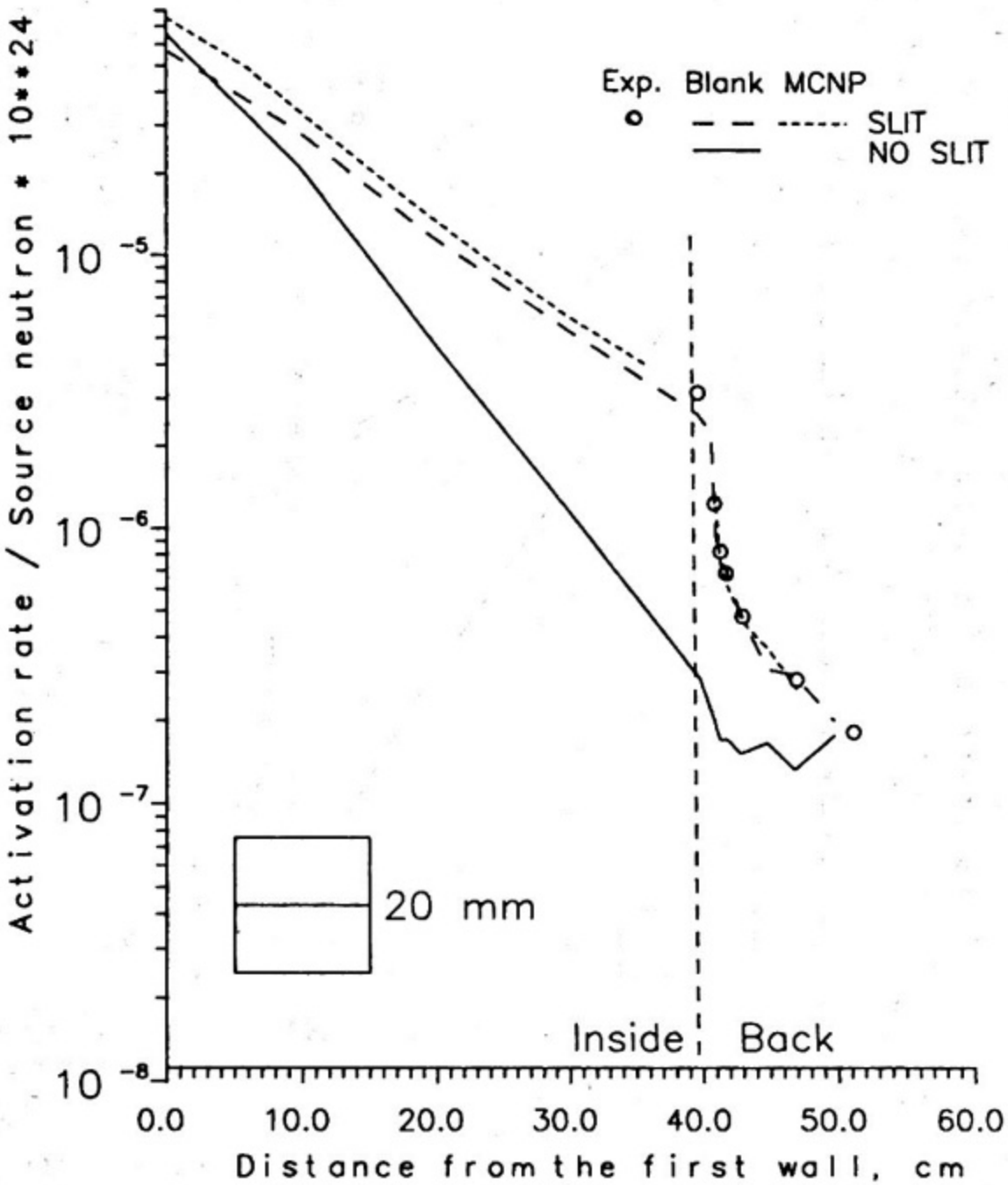

Fig. 33. ^{115}In activation rate distribution in the iron–water assembly with a straight slit 20 mm wide.

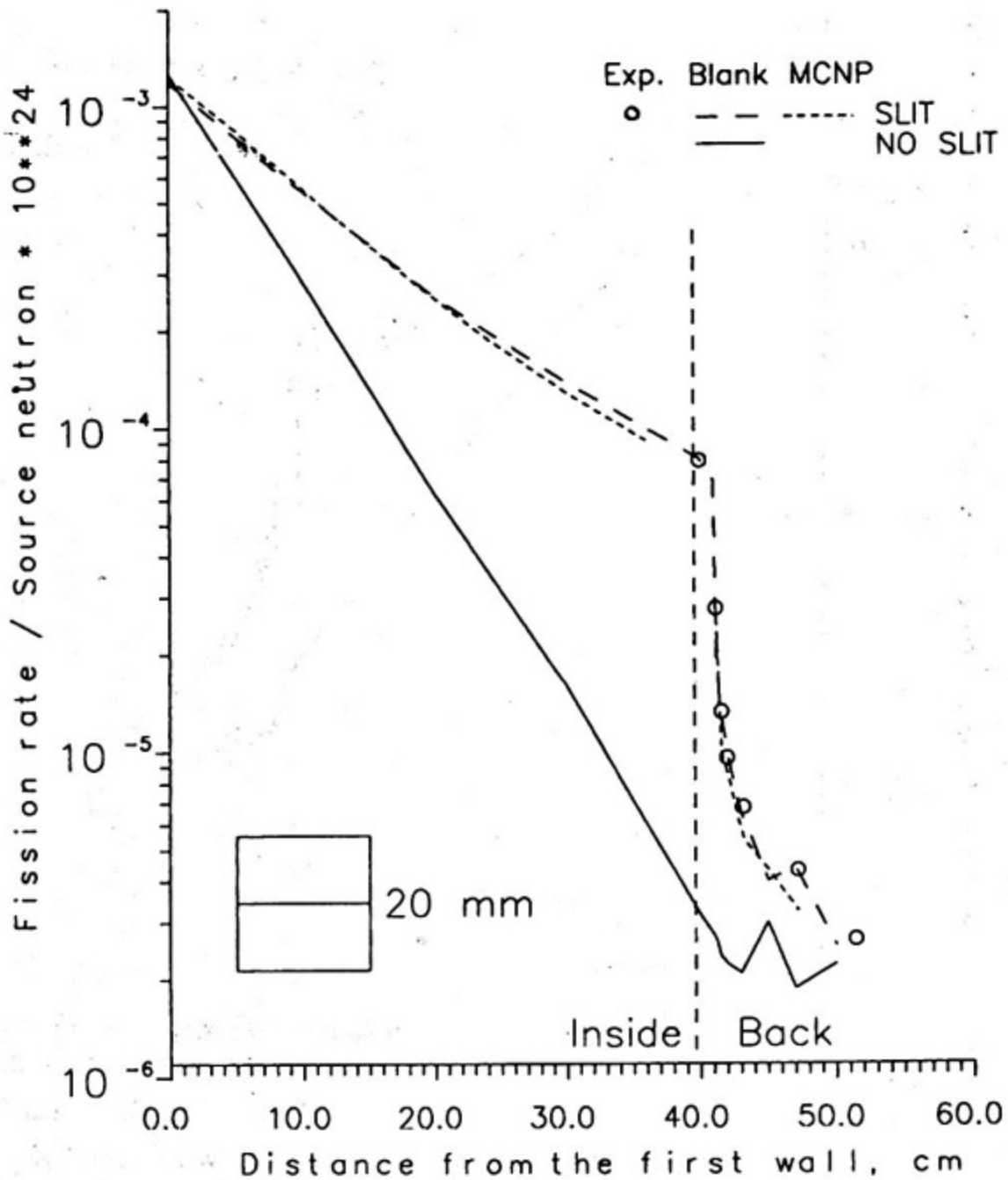

Fig. 34. ^{237}Np fission rate distribution in the iron–water assembly with a straight slit 20 mm wide.

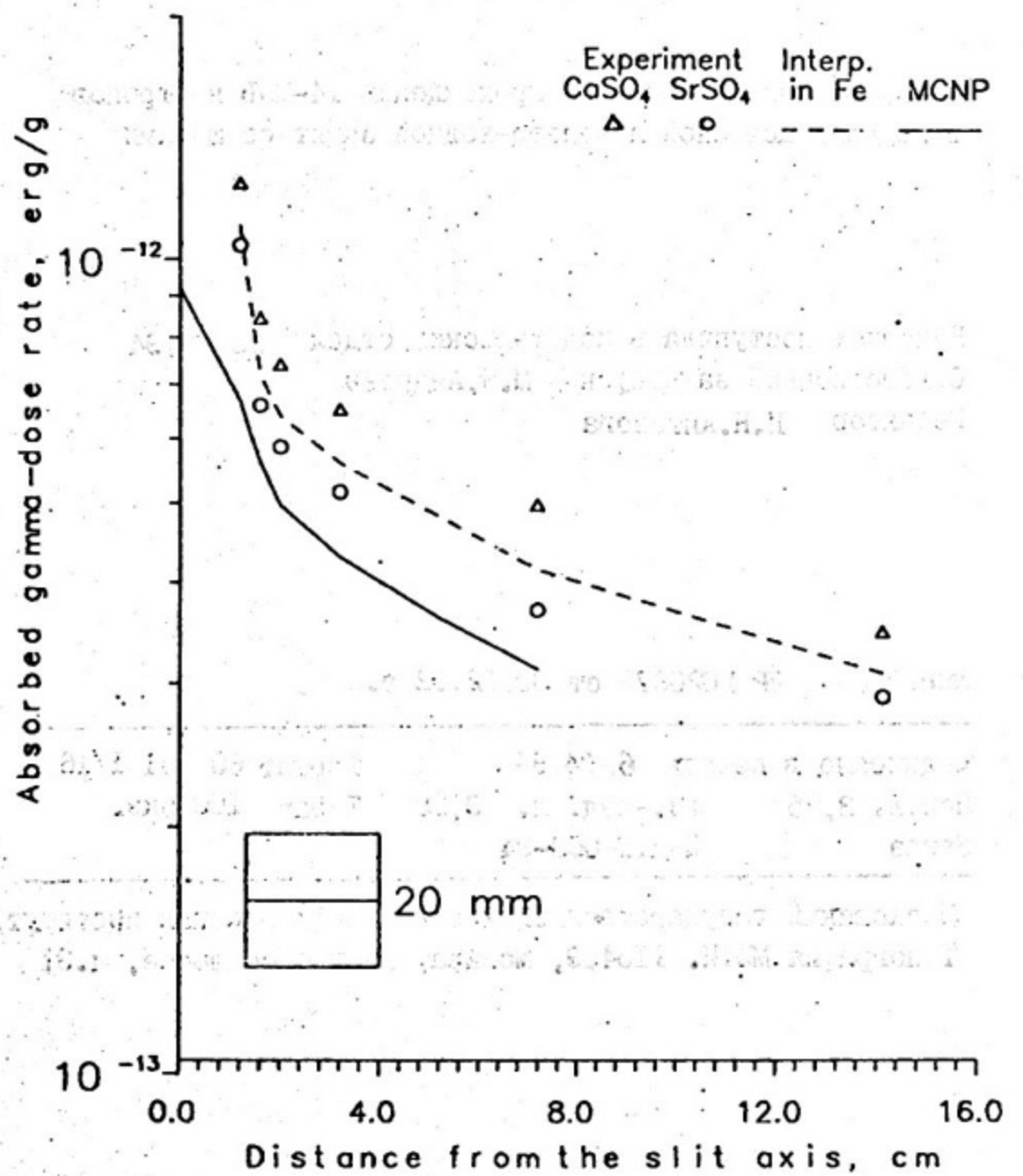

Fig. 35. Gamma-heating rate distribution on the back surface of iron-water mock-up with a straight slit 20 mm wide.

Андреев Михаил Иванович
Афанасьев Валерий Викторович
Белевитин Александр Геннадьевич
Марковский Дмитрий Валентинович
Ромоданов Вадим Леонидович
Свечкопал Андрей Николаевич

Benchmark-эксперимент по прохождению 14-МэВ нейтронов в моделях железной и железо-водной защит со щелями

Рукопись поступила в издательский отдел 25.03.94
Ответственный за выпуск М.И.Андреев
Редактор Н.Н.Антонова

Лицензия ЛР №020676 от 09.12.92 г.

Подписано в печать 6.04.94 Формат 60 84 1/16
Печ.л. 3,25 Уч.-изд. л. 3,25 Тираж 100 экз.
Заказ Изд.№ 003-94

Московский государственный инженерно-физический институт.
Типография МИФИ. 115409, Москва, Каширское шоссе, д.31